nature biotechnology

Article

https://doi.org/10.1038/s41587-024-02267-3

High-yield porphyrin production through metabolic engineering and biocatalysis

Received: 20 August 2023

Accepted: 26 April 2024

Published online: 05 June 2024

Check for updates

Haihong Chen[1,5], Yaohong Wang[1,5], Weishan Wang[2,5], Ting Cao[1,5], Lu Zhang[1,5], Zhengduo Wang[1], Xuran Chi[1], Tong Shi[1], Huangwei Wang[1], Xinwei He[1], Mindong Liang[1], Mengxue Yang[1], Wenyi Jiang[1], Dongyuan Lv[1], Jiaming Yu[1], Guoliang Zhu[1], Yongtao Xie[1], Bei Gao[1], Xinye Wang[1], Xueting Liu[1], Youyuan Li[1], Limin Ouyang[1], Jingyu Zhang[1], Huimin Liu[1], Zilong Li[2], Yaojun Tong[3], Xuekui Xia[4], Gao-Yi Tan[1] ✉ & Lixin Zhang[1] ✉

Porphyrins and their derivatives find extensive applications in medicine, food, energy and materials. In this study, we produced porphyrin compounds by combining *Rhodobacter sphaeroides* as an efficient cell factory with enzymatic catalysis. Genome-wide CRISPRi-based screening in *R. sphaeroides* identifies *hemN* as a target for improved coproporphyrin III (CPIII) production, and exploiting phosphorylation of PrrA further improves the production of bioactive CPIII to 16.5 g L^{-1} by fed-batch fermentation. Subsequent screening and engineering high-activity metal chelatases and coproheme decarboxylase results in the synthesis of various metalloporphyrins, including heme and the anti-tumor agent zincphyrin. After pilot-scale fermentation (200 L) and setting up the purification process for CPIII (purity >95%), we scaled up the production of heme and zincphyrin through enzymatic catalysis in a 5-L bioreactor, with CPIII achieving respective enzyme conversion rates of 63% and 98% and yielding 10.8 g L^{-1} and 21.3 g L^{-1}, respectively. Our strategy offers a solution for high-yield bioproduction of heme and other valuable porphyrins with substantial industrial and medical applications.

Porphyrins are characterized by the interconnection of four pyrrole subunits. Porphyrins constitute a class of heterocyclic compounds showcasing diverse functionalities and wide-ranging applications[1]. Bioactive porphyrins, such as protoporphyrin IX (PPIX) and coproporphyrin III (CPIII), can be used in photodynamic therapy of cancer[2] and treatment of bacterial infections[3,4]. Substituting pyrrole protons with metal ions produces metalloporphyrins, such as naturally occurring chlorophyll, cobalamin (VB_{12}) and heme. These have irreplaceable roles in vital activities and are widely used in the food, feed and medicine industries, among others[5–7]. Moreover, chelation with other transition metals (for example, Mn, Cu and Zn) and incorporating side chain modifications enhance photophysical and electrochemical properties, enabling applications of porphyrin derivatives in energy[8], diagnostics and therapeutics[9]. However, there are major challenges in efficient production of porphyrins. Chlorophyll and heme can be relatively easily separated through chemical extraction from animal or plant tissues[10–12], but the processes involved are environmentally unfriendly and inefficient. Other porphyrins can be obtained only through chemical methods, such as total synthesis or functional derivatization of heme or chlorophyll[13], resulting in low synthesis efficiency and high

[1]State Key Laboratory of Bioreactor Engineering and School of Biotechnology, East China University of Science and Technology, Shanghai, China. [2]State Key Laboratory of Microbial Resources, Institute of Microbiology, Chinese Academy of Sciences, Beijing, China. [3]State Key Laboratory of Microbial Metabolism, School of Life Sciences and Biotechnology, Shanghai Jiao Tong University, Shanghai, China. [4]Key Biosensor Laboratory of Shandong Province, Biology Institute, Qilu University of Technology (Shandong Academy of Sciences), Jinan, China. [5]These authors contributed equally: Haihong Chen, Yaohong Wang, Weishan Wang, Ting Cao, Lu Zhang. ✉e-mail: tangy@ecust.edu.cn; lxzhang@ecust.edu.cn

https://doi.org/10.1038/s41587-024-02267-3

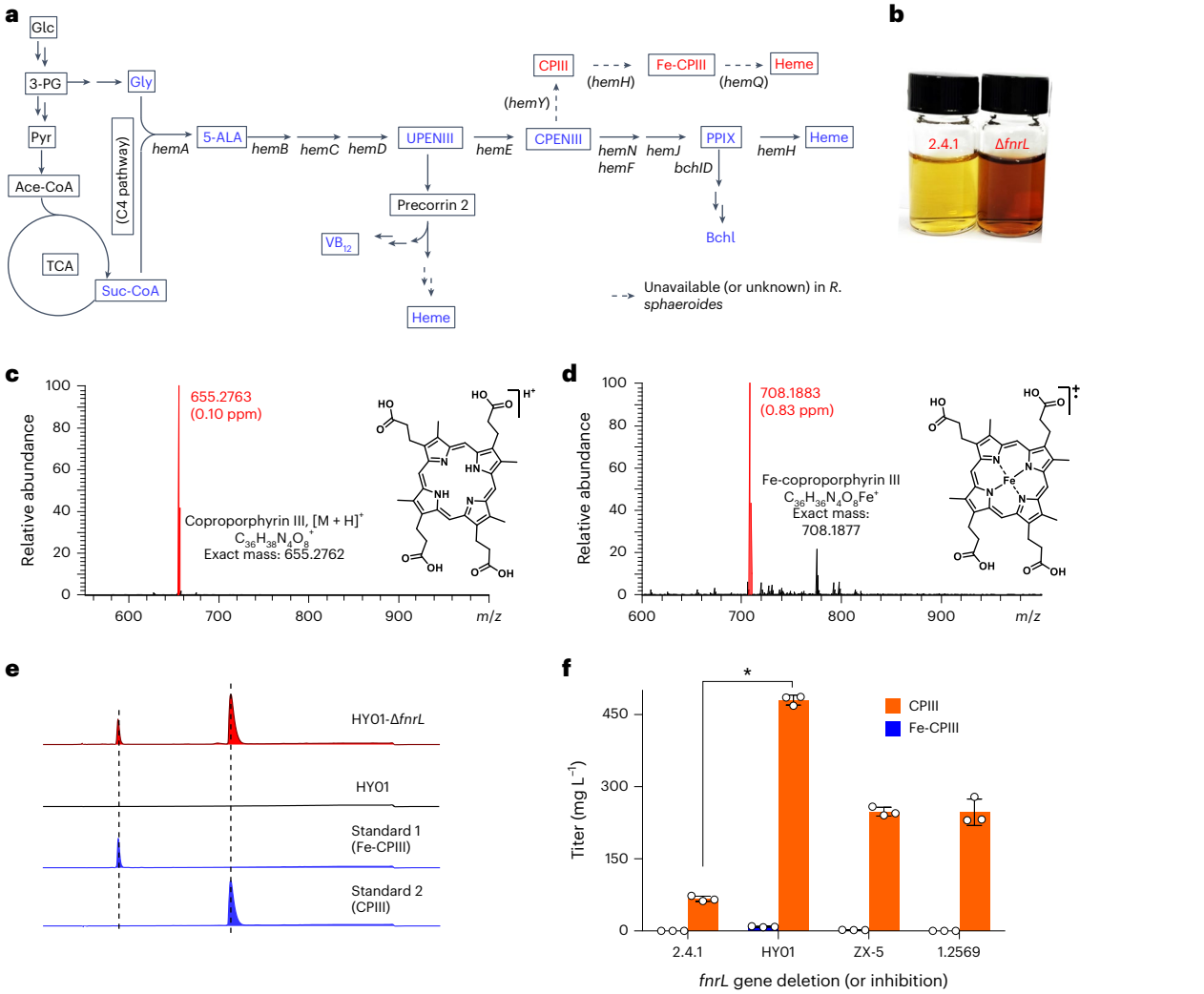


Fig. 1 | Identification and quantitatively analysis of CPIII and Fe-CPIII in different *R. sphaeroides* strains with *fnrL* gene deletion. a, Porphyrin biosynthetic pathway in *R. sphaeroides* 2.4.1. UPENIII, uroporphyrinogen III. **b**, Supernatant fermentation broth of *R. sphaeroides* 2.4.1 and *R. sphaeroides* 2.4.1-Δ*fnrL*. **c**,**d**, Identification of CPIII and Fe-CPIII in fermentation broth of *R. sphaeroides* 2.4.1-Δ*fnrL* by HRMS. **e**, HPLC profile of CPIII and Fe-CPIII in *R. sphaeroides* HY01 and *R. sphaeroides* HY01-Δ*fnrL*. **f**, Analysis of CPIII and Fe-CPIII titer in different *R. sphaeroides* strains with *fnrL* gene deletion (or inhibition) ($n = 3$ biologically independent replicates for each strain). Bar graph with error bars represents mean ± s.d. $^*P < 0.05$.

costs. Therefore, efficient production or synthesis of these porphyrins demands innovative approaches. Bioproduction of these high value-added porphyrins by microbial hosts is attracting increasing attention.

In nature, the porphyrin biosynthesis pathway begins with the synthesis of 5-aminolevulinate (5-ALA). After catalysis to form a tetrapyrrole precursor, it is then further synthesized into various porphyrin compounds (Fig. 1a). In this pathway, key intermediates, such as precomin 2, PPIX and CPIII, can be synthesized into heme through distinct routes[14–16]. Additionally, precorrin 2 and PPIX can respectively serve as precursors for the synthesis of VB_{12} and chlorophyll[17,18]. Early attempts have been made to engineer microorganisms for the synthesis of these porphyrin intermediates. For example, metabolic engineering of *Escherichia coli* and *Shewanella* has been employed to produce PPIX[13,19–21]. It has also been reported that some microorganisms can slightly accumulate CPIII or the anti-tumor agent zincphyrin (namely, Zn-CPIII)[22–25]. *E. coli* was first engineered for secretory production of free heme[26]. Subsequently, other microorganisms, such as *Corynebacterium glutamicum* and *Saccharomyces cerevisiae*, have undergone metabolic engineering to produce heme[27,28]. However, whether it is porphyrin intermediates or heme, the current microbial synthesis efficiency remains remarkably low, with yields typically in the range of milligrams per liter (Supplementary Table. 1). Recently, heme production in *E. coli* was improved to 1 g L^{-1} through fermentation process optimization and supply of feeding solution[7]. Another value-added porphyrin compound, Zn-PPIX, has also been produced by engineered *E. coli*[29].

However, challenges remain in further improving the efficiency of microbial biosynthesis of heme or metalloporphyrins to meet the unmet industrial demands, due to the cellular rigid regulation of the porphyrin pathway and the availability of intracellular metal elements[30–32]. Previous studies reported that certain microorganism can accumulate large amounts of CPIII extracellularly under specific conditions. For instance, in *Arthrobacter hyalinus*, the production of CPIII can reach an impressive 440 mg L^{-1} (ref. 33). Based on these studies, we hypothesized that a microbial cell factory could be constructed for the efficient production of porphyrin intermediates, such as CPIII or PPIX, and subsequent coupling enzyme catalysis in vitro could allow the efficient synthesis of heme, Zn-CPIII or other metalloporphyrins and even various porphyrin derivatives.

In the present study, we focused on the bacterial strain *Rhodobacter sphaeroides*, a purple non-sulfur photosynthetic α-proteobacterium. This bacterium serves as a model organism for photosynthetic research and has great potential as a microbial chassis for the highly efficient

https://doi.org/10.1038/s41587-024-02267-3

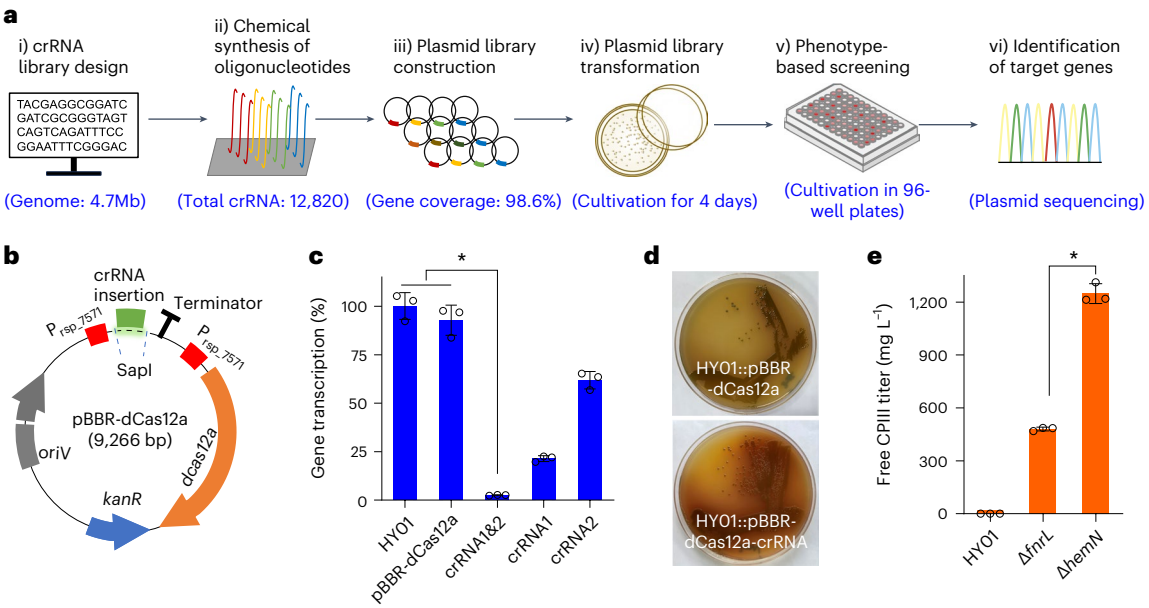


Fig. 2 | Engineering of *R. sphaeroides* HY01 for enhanced CPIII production through CRISPR–dCas12a-derived genome-wide screening. a, Workflow for identifying rate-limiting genes in CPIII biosynthesis through the application of a genome-wide crRNA library. All the crRNA-encoding oligonucleotides are presented in Supplementary Note 2. **b**, Design of the pBBR-dCas12a plasmid for the insertion of crRNA-encoding oligonucleotides. **c**, CRISPRi-mediated gene transcriptional repression in *R. sphaeroides* HY01 ($n = 3$ biologically independent replicates per condition). **d**, The phenotype of HY01::pBBR-dCas12a (control) and HY01::pBBR-dCas12a-crRNA (selected colony) on the agar plate. **e**, Analysis of CPIII yield after deletion of the screened rate-limiting gene ($n = 3$ biologically independent replicates for each strain). Bar graphs with error bars in **c** and **e** represent mean ± s.d. $^*P < 0.05$.

production of coenzyme Q_{10} (refs. 34–38), terpenoids[39–41], hydrogen[42–44] and other compounds. Moreover, various transcriptional regulators, such as the PrrBA two-component activation system and the global anaerobic regulator FnrL, have been well studied to be involved in the regulation of bacteriochlorophyll synthesis and photosynthetic apparatus assembly[45,46]. Previous studies demonstrated that up to 3.6 g L^{-1} of 5-ALA can be produced with high efficiency in *R. sphaeroides* through a reinforced C4 pathway (which converts L-glycine and succinyl-coenzyme A to 5-ALA via ALA synthase)[6,47,48]. Compared to other microbial chassis (for example, *E. coli*, *S. cerevisiae* or *C. glutamicum*), photosynthetic bacteria are naturally more attractive hosts to produce porphyrin intermediates due to their ability to mandatorily synthesize high amounts of tetrapyrrole precursors or bacteriochlorophyll (BChl) in hypoxic or anaerobic conditions[22,49].

We developed an approach for the high-efficient production of porphyrin compounds by combining *R. sphaeroides*-derived cell factory and enzymatic catalysis. *R. sphaeroides* was screened and engineered as a highly efficient microbial cell factory capable of producing extracellular free CPIII. By using CPIII obtained through fermentation, we synthesized various metalloporphyrins through enzymatic catalysis. Throughout this process, we employed a high-throughput (HTP) method to engineer and screen the key enzyme responsible for heme biosynthesis through the CPIII-dependent pathway. Through this approach, we achieved high heme and Zn-CPIII titers in the bioreactor system (Supplementary Table 1), indicating the possibility for cost-efficient, large-scale bioproduction of heme and other value-added porphyrins.

Results

Engineering of *R. sphaeroides* for free CPIII production

CPIII is a key intermediate in the non-canonical CPIII-dependent bacterial heme biosynthesis pathway (Fig. 1a and Extended Data Fig. 1a). *R. sphaeroides* 2.4.1 as a model photosynthetic organism was reported for CPIII production by deletion of the *fnrL* homologous gene[50,51]. Here, a brown pigment was generated in culture broth supernatant of mutant strain 2.4.1-Δ*fnrL* (Fig. 1b and Extended Data Fig. 2a). Subsequent high-resolution mass spectrometry (HRMS) and tandem mass spectrometry (MS/MS) spectra (Extended Data Fig. 1b,c) analyses confirmed the production of free CPIII ($m/z = 655.2763$; $\Delta = 0.10$ ppm) (Fig. 1c). Another compound with $m/z = 708.1883$ ($\Delta = 0.83$ ppm) is Fe-coproporphyrin III (Fe-CPIII), which was also detected by HRMS (Fig. 1d). The production of free CPIII was 66.9 mg L^{-1} in 2.4.1-Δ*fnrL* (Fig. 1f). Fe-CPIII was not quantitatively analyzed by high-performance liquid chromatography (HPLC) due to the low production.

To increase the biosynthetic efficiency of CPIII production, different *R. sphaeroides* subspecies or varieties (that is, *R. sphaeroides* 1.2569, ZX-5 and HY01), which are proficient in producing different products such as coenzyme Q_{10}, terpenoids and hydrogen[34,35,52], were selected as candidate hosts. The *fnrL* homologous gene in these strains was inactivated (or inhibited) for CPIII production (Extended Data Fig. 2b,c). Inactivation of *fnrL* resulted in highly efficient CPIII production (Fig. 1e). The titer reached 480.2 mg L^{-1}, 242.8 mg L^{-1} and 231.5 mg L^{-1} in HY01-Δ*fnrL*, ZX-5-Δ*fnrL* and *R. sphaeroides* 1.2569-*fnrL*$_i$ (*fnrL* inhibition), respectively (Fig. 1f). Compared to 2.4.1-Δ*fnrL*, the production of CPIII in HY01-Δ*fnrL* increased 6.2-fold ($P < 0.05$), and the production of free Fe-CPIII reached 8.6 mg L^{-1}. These results implicate HY01 as a promising host for CPIII production.

Genome-wide CRISPR interference screening for CPIII overproduction

The production of free CPIII can lead to a reddish-brown color in the fermentation broth (Fig. 1b), which is an intuitive phenotype for screening strains. Therefore, to further enhance CPIII production, we developed a CRISPR–dCas12a-based HTP method to find or identify bottlenecks in CPIII overproduction (Fig. 2a). Before this, we initially established and characterized a dCas12a-based CRISPR interference (CRISPRi) system in HY01. The high-activity promoter P_{rsp_7571} (ref. 35) was used to control the transcription of both the dCas12a gene and CRISPR RNA (crRNA) (Fig. 2b). When crRNA targeted the 5′ untranslated region or when two

https://doi.org/10.1038/s41587-024-02267-3

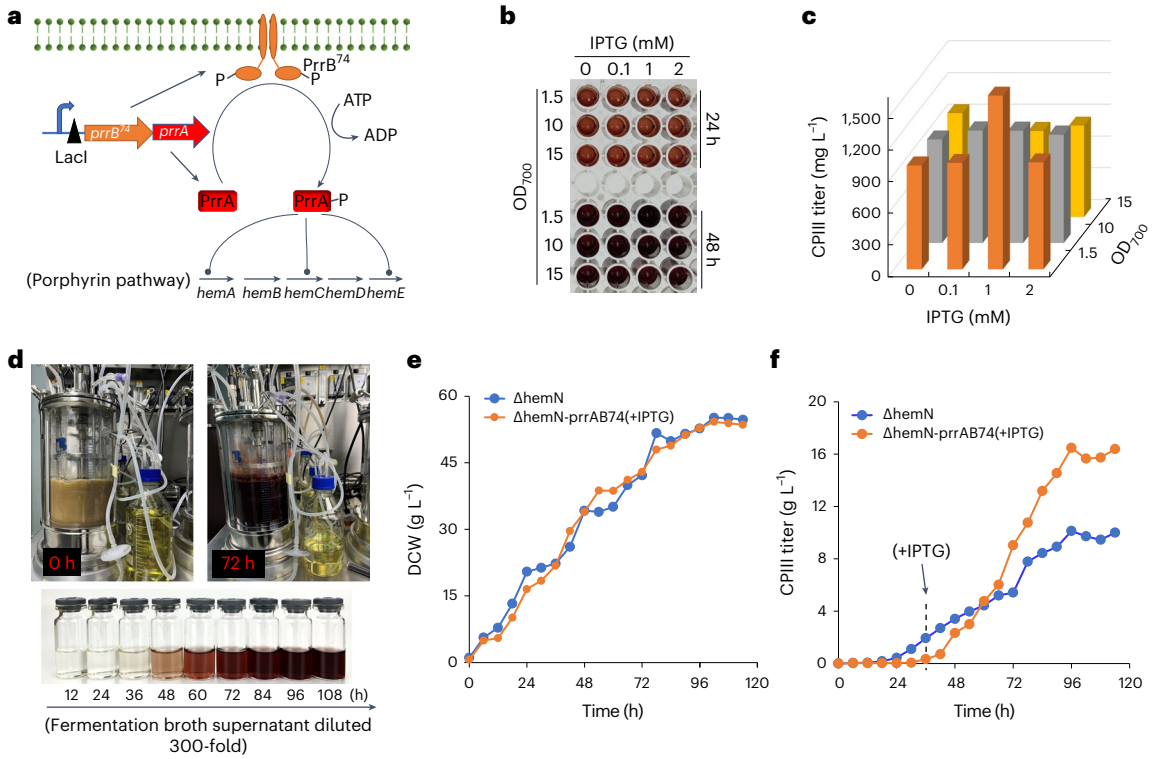


Fig. 3 | Fine-tune timing of PrrA phosphorylation boosts CPIII production in a 5-L bioreactor. a, Rewiring the phosphorylation pathway of *prrA* through the histidine kinase mutant $PrrB_{pLB2}$. **b**,**c**, Timing of PrrA phosphorylation for CPIII overproduction using IPTG in *R. sphaeroides* HY01-Δ*hemN-prrAB*$_{pLB2}$. IPTG was added to the final concentration of 0 mM, 0.1 mM, 1 mM and 2 mM at OD of 1.5, 10 and 15. At 24 h and 48 h of fermentation, samples were taken for observing the color of the fermentation broth and measuring the concentration of CPIII. **d**, Fed-batch *R. sphaeroides* HY01-Δ*hemN* culture in the 5-L bioreactor. **e**,**f**, Enhanced CPIII production in fed-batch culture of *R. sphaeroides* HY01-Δ*hemN-prrAB*$_{pLB2}$ by IPTG induction. Based on the transcription timecourse of PrrA target operons (Extended Data Fig. 2f), IPTG was introduced into the bioreactor after 36 h of fermentation, reaching a final concentration of 1 mM.

crRNAs were used, the inhibition rate of the target gene exceeded 90% ($P < 0.05$) (Fig. 2c).

As shown in Fig. 2a, a genome-wide crRNA library was designed and synthesized (Supplementary Note 1). The oligonucleotides encoding crRNA were then assembled with pBBR-dCas12a plasmids (Fig. 2b) to obtain a corresponding plasmid library (Supplementary Table. 2). After transformation of the plasmid library into HY01, colonies with noticeable color phenotype changes were selected for next-step fermentation in 96-well plates. Then, a colony that produced a large amount of pigment was selected (Fig. 2d). Subsequent sequencing indicated that the crRNA targeted a gene encoding coproporphyrinogen III (CPENIII) oxidase, which was designated *hemN*. This result indicated that inhibiting the transcription of *hemN* is favorable for CPIII production, as the oxygen-independent CPENIII oxidase encoded by *hemN* consumes CPENIII, thereby hindering CPIII formation. When *hemN* was inactivated, the free CPIII titer reached 1,250 mg L^{-1}, representing a 160% ($P < 0.05$) improvement compared to *fnrL* knockout (Fig. 2e and Extended Data Fig. 2d).

Timing PrrAB regulation and fed-batch boost CPIII production

The PrrAB two-component system in *R. sphaeroides* was reported as a toggle for the porphyrin metabolic pathway[45]. Previously, PrrA was employed as a regulatory activator to enhance lycopene production through overexpression[53]. It was also reported that specific mutations of the histidine kinase PrrB (for example, $PrrB_{pLB2}$) can hijack the phosphorylation process of response regulator PrrA[54]. In this study, the regulatory circuit was rewired using LacI and $PrrB_{pLB2}$ to achieve fine-tune timing of PrrA phosphorylation using isopropyl β-D-1-thiogalactopyranoside (IPTG) (Fig. 3a and Extended Data Fig. 2e). After optimizing the induction time (OD) and inducer concentration, the titer of free CPIII reached 1,640 mg L^{-1} (Fig. 3b,c), which was more than 31% higher than that of HY01-Δ*hemN*. We subsequently tested the fermentation performance of the strains in 5-L stirred bioreactors (Fig. 3d). Using a glucose fed-batch strategy, the titer of free CPIII in HY01-Δ*hemN* reached 10.1 g L^{-1} after 96 h of fermentation (Fig. 3e,f). Following the same fed-batch strategy and considering the transcription timecourse of *prrA*'s regulon within the bioreactor, which includes genes such as *hemA*, *hemC* and *hemE*[46] (Fig. 1a and Extended Data Fig. 2f), this study added IPTG at 36 h of fermentation. It was found that the production of free CPIII finally reached 16.5 g L^{-1} in HY01-Δ*hemN-prrAB*$_{pLB2}$ (Fig. 3e,f). Thus far, through engineering and optimization, the production of CPIII has been gradually increased (Extended Data Fig. 2g), and *R. sphaeroides* has been transformed into an efficient microbial cell factory to produce CPIII.

Convert CPIII to metalloporphyrin compounds by biocatalysis

Fe-CPIII, also known as coproheme III, serves as the precursor of heme biosynthesis[55]. Fe-CPIII can be converted to heme by removing two carboxyl groups (Fig. 4a). To establish an efficient route for Fe-CPIII production, we compared and evaluated the ferrochelatase (HemH) activity from various sources. HemH from *Staphylococcus aureus* ($HemH_{Sa}$) demonstrated remarkably superior activity compared to the other enzymes ($P < 0.05$; Fig. 4b). In the presence of Fe^{2+}, $HemH_{Sa}$ efficiently converted CPIII to Fe-CPIII (Fig. 4d). CPIII and $HemH_{Sa}$ were also used to synthesize other kinds of metalloporphyrins by adding corresponding metal ions, such as Co-CPIII, Mn-CPIII, Ni-CPIII and Cu-CPIII, with substrate conversion rates reaching 100%. Co^{2+}, Mn^{2+} and Cu^{2+} could spontaneously react with CPIII to produce metalloporphyrins specific to each metal ion (Fig. 4c,d and Extended Data Fig. 3a–d). In addition, Zn-CPIII as a CPIII-derived metalloporphyrin (Fig. 4c) has advantages

https://doi.org/10.1038/s41587-024-02267-3

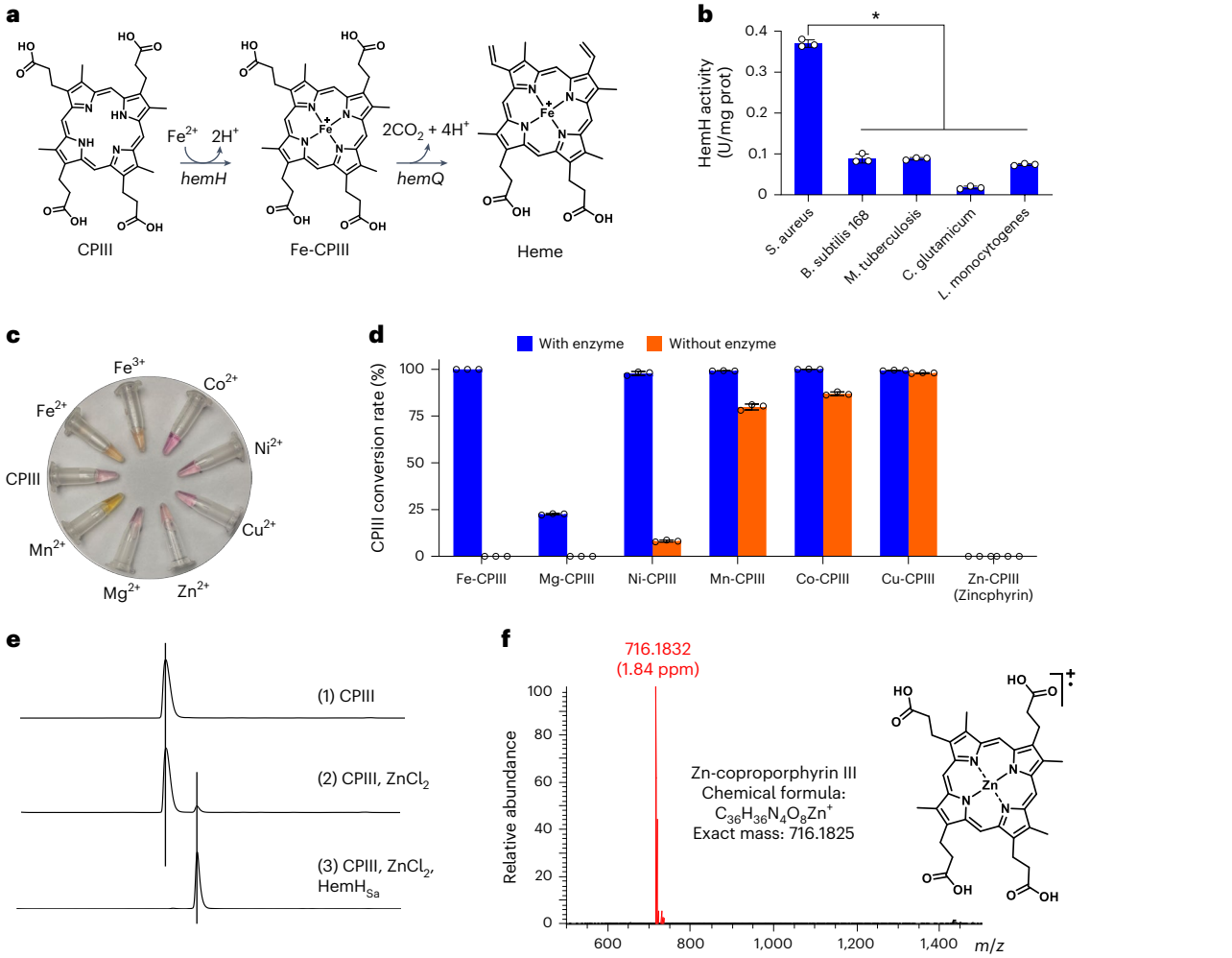


Fig. 4 | In vitro biosynthesis of metalloporphyrins by enzymatic catalysis. **a**, In vitro biosynthesis of heme through the CPIII-dependent pathway. **b**, Analysis of the ferrochelatase (HemH) activity from various microorganisms ($n = 3$ biologically independent enzymatic activity detection experiments for each HemH homolog). Various HemH derived from *S. aureus*, *Bacillus subtilis*, *Mycobacterium tuberculosis*, *C. glutamicum* and *Listeria monocytogenes* were used. **c**,**d**, Biosynthesis of Fe-CPIII and other different metalloporphyrins using CPIII and HemH derived from *S. aureus* ($n = 3$ biological replicates per condition). All the resulting metalloporphyrins were verified by HRMS (Extended Data Fig. 3a–d). **e**, HPLC profile of the enzymatic catalysis of CPIII for the in vitro synthesis of Zn-CPIII using $HemH_{Sa}$ and zinc chloride. The reaction is conducted in Tris-HCl buffer (pH 7.0) at 37 °C under the following conditions. (1) In the reaction system, only CPIII is present. (ii) In condition (1), $ZnCl_2$ is added. (3) In condition (2), $HemH_{Sa}$ is added. **f**, Verification of Zn-CPIII production by HRMS. Bar graphs with error bars in **b** and **d** represent mean ± s.d. $^*P < 0.05$.

over other porphyrins as a practical photodynamic therapy reagent[56,57]. In the present study, we found that, using $HemH_{Sa}$ and zinc sulfate, CPIII could not be converted to Zn-CPIII (Fig. 4d and Extended Data Fig. 3e). After comparing different zinc salts, including zinc acetate, zinc sulfate and zinc chloride, we found that zinc chloride can spontaneously react with CPIII but with relatively low activity (Fig. 4e). However, after adding $HemH_{Sa}$, within 10 min, CPIII is completely converted into Zn-CPIII (Fig. 4e,f). These findings suggest that the subsequent use of in vitro enzymatic catalysis can enable efficient production of Zn-CPIII and other kinds of metalloporphyrin compounds.

Engineering coproheme decarboxylase for heme biosynthesis

Heme is another extensively studied metalloporphyrin, which is also an essential component that imparts a meaty flavor and aroma to plant-based meat products[58]. We, therefore, aimed to establish an efficient route for heme biosynthesis by applying CPIII. However, the coproheme decarboxylase (HemQ)[55] responsible for decarboxylating Fe-CPIII to generate heme is limited by its low activity (Fig. 4a), which hinders efficient heme production. To overcome this, a CRISPR–Cas12a-based detection method was designed to screen high-activity HemQ by detecting heme. As shown in Fig. 5a, the method employs an allosteric transcription protein, HrtR, derived from *Lactococcus lactis*[59]. This protein can bind to and sense heme and has been used as an in vivo biosensor for heme monitoring[60]. In this study, HrtR was immobilized on a microplate via biotin–streptavidin affinity[61]. After immobilization, the DNA-binding domain (DBD) of the HrtR can bind to double-stranded DNA (dsDNA) containing HrtR's binding motif, forming a DNA–protein complex. Heme can bind to the effector-binding domain (EBD) of the HrtR, causing the dissociation of the DNA–protein complex, thereby releasing dsDNA. By designing crRNA targeting this dsDNA, the indiscriminate single-stranded DNA (ssDNA) cleavage activity of CRISPR–Cas12a can be activated, further cleaving an ssDNA probe labeled with a fluorophore quencher (FQ) and producing fluorescence[62]. Ultimately, the detection of fluorescence enables the detection of heme.

To establish the screening system, we tested the effect of biotinylation on the DNA binding activity of HrtR and its allosteric activity induced in an electrophoretic mobility shift assay (EMSA). Biotinylated HrtR (Biot-HrtR) had strong binding activity with dsDNA, and there was a dose–response relationship between the formation of HrtR–dsDNA complex and the concentration of Biot-HrtR (Fig. 5b). Heme could

https://doi.org/10.1038/s41587-024-02267-3

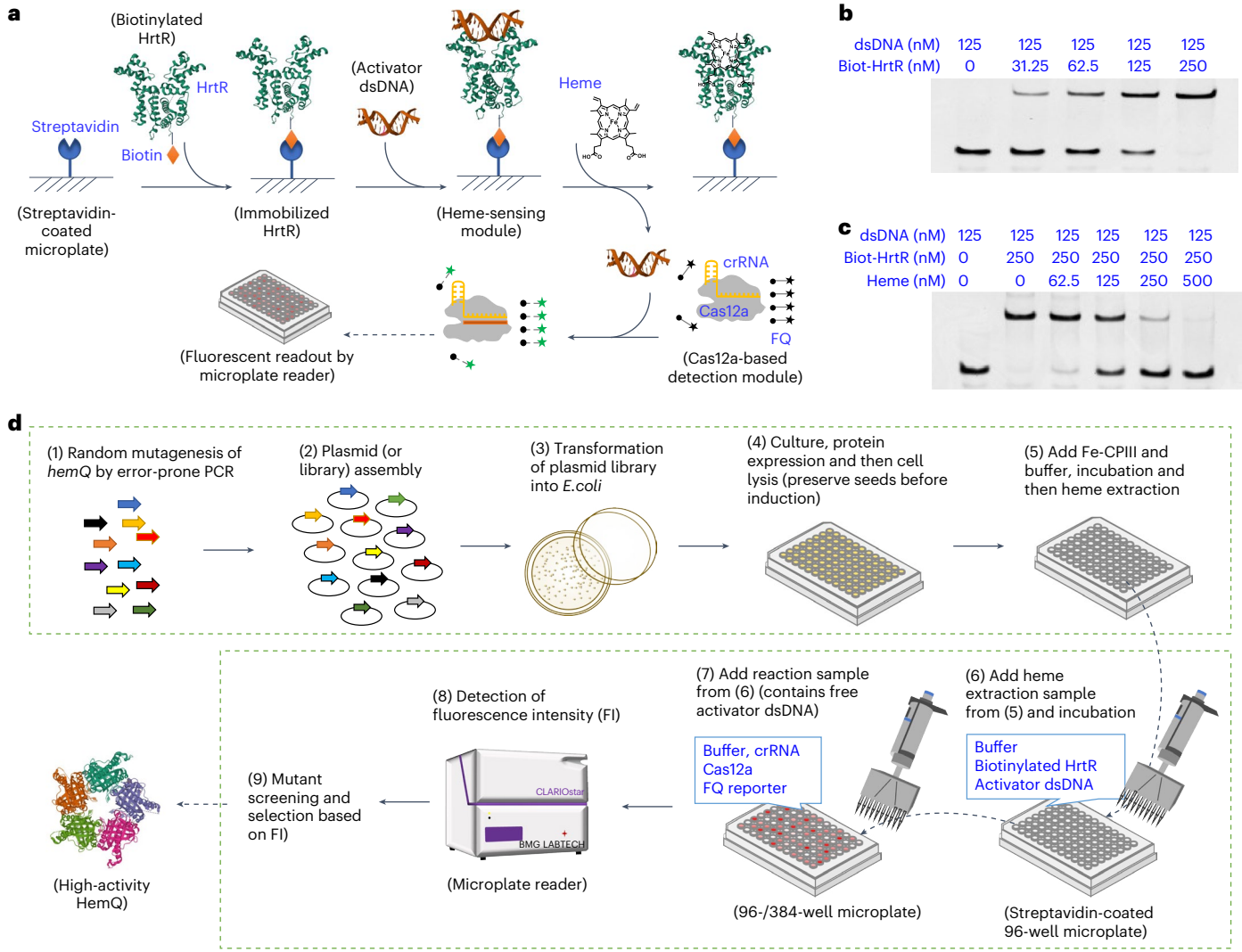


Fig. 5 | Screening and engineering HemQ for efficient conversion of CPIII to heme. a, Schematic diagram of CRISPR–Cas12a-derived biosensing strategy for HTP detection of heme. **b**, EMSA with Biot-HrtR and dsDNA containing the HrtR-binding motif. **c**, EMSA evaluation of Biot-HrtR allosteric activities in the presence of heme. The EMSA assays in **b** and **c** were respectively performed three times ($n = 3$; replicates are shown in Source Data files). **d**, Workflow for screening and engineering HemQ by high-throughput heme detection. **e**, Michaelis–Menten plot for different HemQ conversions of Fe-CPIII to heme. Measured K_m and k_{cat} values are reported as mean ± s.d., with three replicates. V_o, rate of catalysis. **f**, Comparative analysis of crude enzyme activity for $HemQ_{Sa}$, $HemeQ_{28}$ and $HemeQ_{28-M}$ ($n = 3$ biologically independent replicates for each HemQ homolog or mutant). **g**, HPLC profile of the enzymatic catalysis of CPIII for the synthesis of heme in vitro. Bar graph with error bars represent mean ± s.d. *$P < 0.05$.

cause the dissociation of HrtR–dsDNA complex, and, with increasing heme concentration, more dsDNA was released (Fig. 5c). This method specifically responded to heme, with no response to other porphyrin compounds (for example, CPI, CPIII, Fe-CPIII and PPIX) (Extended Data Fig. 4a). Using this method, heme at the nanomolar level (linear detection range: 10–200 nM, $R^2 > 0.99$; Extended Data Fig. 4b) can

https://doi.org/10.1038/s41587-024-02267-3

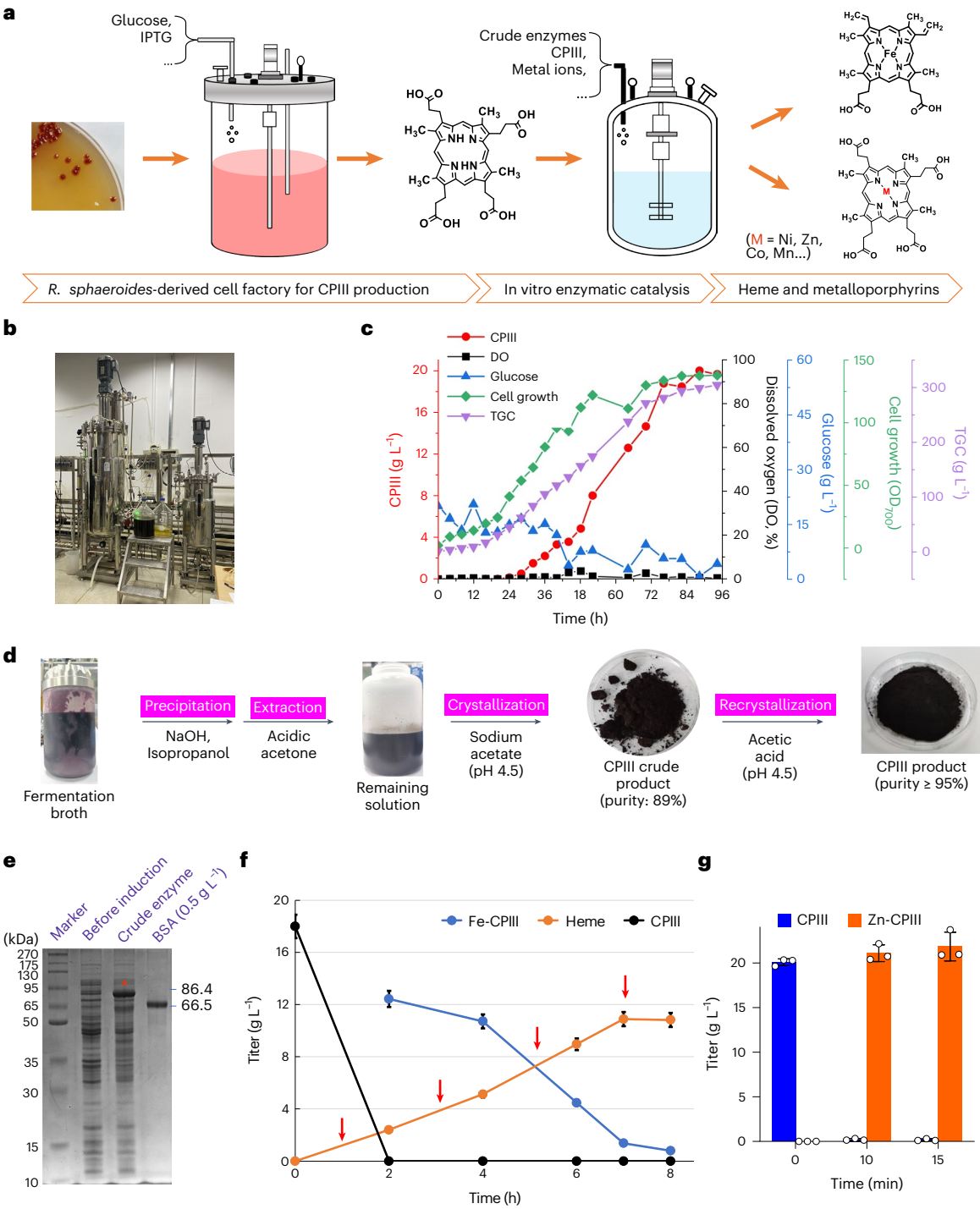


Fig. 6 | Bioproduction of heme and Zn-CPIII in a 5-L bioreactor. a, Schematic diagram of the manufacture of various porphyrins by combining enzymatic catalysis and *R. sphaeroides*-derived cell factory. **b**,**c**, Fed-batch fermentation of CPIII in a 200-L bioreactor. The timecourse of CPIII titer, cell growth, total glucose consumption (TGC) and dissolved oxygen (DO) was monitored in a 200-L bioreactor. **d**, Purification and preparation of CPIII from cultivated *R. sphaeroides* by recrystallization. **e**, SDS-PAGE analysis of lysate supernatant from recombinant *E. coli* cells, with induction (namely, crude enzyme) or before induction. The $HemH_{Sa}$ and $HemQ_{28\text{-}M}$ fusion protein (86.4 kDa) is indicated by a star (*). BSA (0.5 mg ml^{-1}) was used as reference (66.5 kDa). The SDA-PAGE assay in **e** was performed three times ($n = 3$; replicates are shown in Source Data files). **f**, Batch-wise addition of crude enzyme catalyzed the conversion CPIII to heme in a 5-L bioreactor. At the beginning of the reaction, 2 L of CPIII with a concentration of 18 g L^{-1} was added all at once. As shown by the arrow in the diagram, the crude enzyme supernatant obtained by crushing 180 g of wet recombinant *E. coli* cells was added to the reaction system at five different timepoints: 0 h, 1 h, 3 h, 5 h and 7 h. The reaction was performed at 37 °C and pH 7.0 with agitation at 100 r.p.m. Error bars in **f** represent s.d. of three independent replicates. **g**, Biosynthesis of Zn-CPIII through in vitro transformation of CPIII. One liter of CPIII with a concentration of 20 g L^{-1} was used for catalytic reaction illustration. Zinc chloride and crude enzyme (obtained by crushing 30 g of wet recombinant *E. coli* cells) were added to the bioreactor at the beginning of the reaction. The reaction was conducted at room temperature and pH 7.0 with agitation at 100 r.p.m. The blue bars at 10 min and 15 min correspond to CPIII concentrations of 0.23 ± 0.11 g L^{-1} and 0.20 ± 0.11 g L^{-1}, respectively. $n = 3$ biologically independent replicates for each data point in **f** and **g**. Bar graphs with error bars represent mean ± s.d.

be rapidly detected, with a coefficient of variation not exceeding 6% and a detection recovery rate exceeding 98% (Extended Data Fig. 4c). These results indicate the good stability and robustness of the method in detecting heme.

An HTP method for screening high-activity HemQ was developed (Fig. 5d). Using this method, a highly active protein, designated as $HemQ_{28}$ and originating from *Alicyclobacillus sacchari*, was successfully screened from 31 selected HemQ homologous proteins (Extended Data Fig. 5a and Supplementary Table. 3). $HemQ_{28}$ exhibited a 2.2–60.9-fold increase in enzyme catalytic activity (U/mg prot) compared to previously reported HemQ homologs (Extended Data Fig. 5b). Subsequently, a random mutant library based on $hemQ_{28}$ was constructed using error-prone polymerase chain reaction (PCR). After screening the library from approximately 11,000 clones using the method illustrated in Extended Data Fig. 6, a variant named $HemQ_{28\text{-}M}$ (Supplementary Note 3) was obtained, which exhibited over a two-fold increase in catalytic activity. Compared to the previously reported highest-activity $HemQ_{Sa}$, $HemQ_{28\text{-}M}$ exhibited a 4.9-fold increase in k_{cat}/K_m and a 10-fold increase in enzyme activity ($P < 0.05$; Fig. 5e,f). Next, the catalytic efficiency of $HemH_{Sa}$ and $HemQ_{28\text{-}M}$ proteins to convert CPIII into heme was examined. As shown in Fig. 5g, when CPIII was incubated with $HemH_{Sa}$, $HemQ_{28\text{-}M}$ and Fe^{2+}, most of the Fe-CPIII was converted to heme. Quantitative analysis revealed that the conversion of CPIII to heme reached 75%, with a small amount of the intermediate harderoheme III (ref. 63) remaining unconverted apart from CPIII (Extended Data Fig. 7a,b). These results suggest that, by combining an in vitro enzymatic catalysis with high-yield CPIII fermentation, a route for efficient heme production could be established.

Pilot-scale fermentation and purification of CPIII

To demonstrate the scale-up potential of the synthesis of heme, Zn-CPIII and other metalloporphyrins by combining *R. sphaeroides*-derived cell factory and in vitro enzymatic catalysis, this study proposes the workflow as shown in Fig. 6a. To achieve a sufficient amount of CPIII for subsequent enzymatic synthesis of heme and Zn-CPIII, this study further scaled up the fermentation of CPIII in a 200-L pilot bioreactor (Fig. 6b). Owing to the improvements in dissolved oxygen supply, the production of CPIII reached 19.6 g L^{-1} (Fig. 6c). Given the high extracellular CPIII concentration in the fermentation broth and its solubility, we investigated direct crystallization for CPIII preparation and purification, and a purification and preparation process was developed, as illustrated in Extended Data Fig. 8a. We found that employing alkali precipitation and isopropanol precipitation, followed by extraction with acidic acetone, improved the recovery rate and purity of CPIII, reaching 90% and 86%, respectively (Extended Data Fig. 8b,c). To further enhanced purity, this study fine-tuned crystallization conditions and performed recrystallization, resulting in CPIII purity exceeding 95% and a recovery rate of approximately 88% (Extended Data Fig. 8d–k). These results indicate that CPIII can be produced in large amounts at a low cost. These results further indicate that CPIII can be readily produced in large amounts, suggesting its great potential for large-scale production.

Scale-up bioproduction of heme and Zn-CPIII

Subsequently, this study demonstrated the use of CPIII prepared through fermentation and recrystallization for the scale-up bioproduction of heme and Zn-CPIII in a 5-L stirred tank bioreactor. A recombinant protein comprising a fusion of $HemH_{Sa}$ and $HemQ_{28\text{-}M}$ (Fig. 6e) was constructed and expressed for catalyzing the synthesis of heme. By using a 5-L bioreactor, we initially tested a one-time batch feed of CPIII, Fe^{2+} and the crude enzyme solution (CES). After 16 h of enzymatic catalysis, we observed that CPIII was completely converted to Fe-CPIII. However, the heme yield was only 3.0 g L^{-1}, with a CPIII conversion rate of 17.8%, accompanied by a large amount of Fe-CPIII accumulation. Consequently, we used a one-time addition of CPIII and Fe^{2+}, followed by a fed-batch addition of the CES every 2 h after the reaction commenced, to maintain the coproheme decarboxylase catalytic activity in the reaction system (Extended Data Fig. 7e). After 7 h of enzymatic catalysis, heme yield reached 10.8 g L^{-1}, and the conversion rate of CPIII reached 64% (Fig. 6f). In addition, the Zn-CPIII was also be readily biosynthesized on a larger scale. A catalytic yield of 21.3 g L^{-1} Zn-CPIII could be achieved with 98% conversion of CPIII in a 1-L reaction volume (Fig. 6g).

Lastly, a techno-economic analysis was conducted to simulate the financial feasibility of scaling up CPIII and heme production. Based on the data obtained from our pilot-scale and purification process, as well as relevant cost data (Supplementary Table. 4), an industrial model for producing heme (or CPIII) at an annual scale exceeding 10 tons was simulated using SuperPro Designer version 10.7 software (Extended Data Fig. 9 and Supplementary Table. 5). The comprehensive cost-effectiveness analyses provided insights into the large-scale production costs, including annual operating expenses encompassing fermentation costs, CPIII isolation and purification, preparation and addition of CES as well as heme preparation (Extended Data Fig. 10a). The minimum product selling price (MPSP, in 2024 dollars with an internal rate of return of 10.1%) for heme and CPIII is $205 per kilogram and $67.5 per kilogram, respectively (Supplementary Table. 5). These results demonstrate the economic viability of bioproducing highly valued porphyrin compounds, such as heme and CPIII, highlighting the substantial potential of our developed route for biomanufacturing various other metalloporphyrin compounds.

Discussion

In this study, we chose photosynthetic purple bacteria, which are distinctly advantageous in porphyrin metabolism compared to non-photosynthetic bacteria. The synthesis of BChl in these bacteria is directly associated with cell survival or growth under specific conditions[64], presenting an opportunity for further engineering aimed at the production of value-added porphyrins. Notably, the non-canonical CPIII-dependent heme biosynthesis pathway is absent in HY01 (Fig. 1a). However, upon *fnrL* deletion, there was an accumulation of CPIII and Fe-CPIII in the different strains (Fig. 1b–f). The deletion of *fnrL* leads to inhibition of PPIX and BChl biosynthesis, resulting in the accumulation of CPENIII (ref. 22). The accumulation of CPIII is thought to be the result of the spontaneous oxidation of CPENIII (ref. 65). Concerning the accumulation of Fe-CPIII, we speculate that it is due to the catalytic activity of protoporphyrin ferrochelatase in the canonical heme biosynthesis pathway[66]. Furthermore, HY01 exhibits a higher capacity for CPIII production compared to other bacteria (Fig. 1f). The main reason may be attributed to HY01 being a high-yield producer of coenzyme Q_{10}. During the screening of coenzyme Q_{10} high-yield producers, the biosynthesis pathway of BChl is simultaneously reinforced[67], resulting in an increased metabolic flux across the entire porphyrin pathway. The mechanism underlying this phenomenon is still being investigated.

When we used the CRISPRi strategy to screen for the bottleneck gene that limits CPIII production, the *hemN* gene was identified (Fig. 2). Two types of CPENIII oxidase, HemF and HemN, were identified in *R. sphaeroides*[50,68]. HemN functions as an oxygen-independent CPENIII oxidase and is expressed only under low oxygen conditions. HemN is responsible for converting CPENIII into protoporphyrinogen IX, which is subsequently decarboxylated to PPIX for BChl biosynthesis[15]. In this study, deletion (or inhibition) of *hemN* impeded and hijacked the precursors originally meant for BChl biosynthesis, leading to a considerable accumulation of CPIII. Previous studies indicated that, under oxygen-limited conditions, *hemN* transcription is positively regulated by *fnrL*[69]. In other words, the observed accumulation of CPIII after the *fnrL* deletion is most likely due to the inhibition of *hemN* transcription. Furthermore, the inactivation of *fnrL* hampers the expression of genes related to the respiratory chain and the synthesis of tetrapyrrole precursor 5-ALA[46]. This explains why there is a higher accumulation of CPIII in the *hemN* mutant compared to the *fnrL* mutant.

The rapid efflux of CPIII (also possibly CPENIII) can relieve feedback inhibition within the cell. Therefore, in fed-batch fermentation (Fig. 3d–f), a yield of CPIII of up to 10 g L^{-1} becomes feasible. Furthermore, the timing of porphyrin pathway expression is related to the yield of CPIII (Fig. 3a–c). Notably, PrrAB, as a two-component global regulatory system involved in oxygen and photosynthesis gene regulation[70], can sense the cellular redox state and activate the porphyrin pathway by controlling the expression of *hemA*, *hemC* and *hemE*[46]. However, under aerobic conditions, overexpressing *prrA* or untimely transcriptional upregulation may detrimentally affect cell growth. In this study, manipulating PrrA phosphorylation using $PrrB_{pLB2}$ (ref. 71) and timely inducing PrrA phosphorylation with IPTG can significantly increase extracellular free CPIII production, which can reach 16.5 g L^{-1} (Fig. 3f).

The efficient production of free CPIII serves as the central hub for the relay synthesis of downstream metalloporphyrins. $HemH_{Sa}$, acting as high-activity Fe^{2+} chelating enzyme for CPIII (Fig. 4a,b), is capable of indiscriminately chelating certain metal ions onto the porphyrin ring, including Ni^{2+}, Mn^{2+}, Co^{2+}, Cu^{2+} and Zn^{2+} and others (Fig. 4c–f). To demonstrate the scale-up potential of metalloporphyrins bioproduction, value-added heme and Zn-CPIII were selected as examples. However, for heme production, the activity of the reported HemQ is too low to meet the requirements of in vitro enzyme catalysis[16]. Therefore, we employed a self-developed screening method to obtain a highly active $HemQ_{28\text{-}M}$ protein through enzyme mining and mutagenesis screening (Fig. 5a). Compared to $HemQ_{Sa}$, $HemQ_{28\text{-}M}$ exhibited over a 10-fold increase in activity as well as enhanced the thermal and acid stability (Extended Data Fig. 7c,d). By combining $HemH_{Sa}$ and $HemQ_{28\text{-}M}$, the yield of heme from CPIII could exceed 75%. We subsequently engineered a fusion protein of $HemH_{Sa}$ and $HemQ_{28\text{-}M}$, which simplified the operations and significantly enhanced the expression level of $HemQ_{28\text{-}M}$. Combined with feed addition of crude enzyme, a heme yield of 10.8 g L^{-1} was achieved in a 5-L bioreactor (Fig. 6). To our knowledge, this is the highest yield achieved to date using biological methods. Notably, a portion of Fe-CPIII remains unconverted, and a small amount of catalytic intermediates are present[15]. Further modifications to $HemQ_{28\text{-}M}$ can be implemented to enhance its catalytic efficiency. Our findings indicate that CPIII can efficiently chelate Zn^{2+} to achieve the synthesis of Zn-CPIII under enzymatic conditions. With enzymatic catalysis, a yield of 21.3 g L^{-1} Zn-CPIII was achieved in a 5-L reactor (Fig. 6). This efficient and cost-effective method of Zn-CPIII production paves the way for future industrial applications.

The pilot-scale CPIII fermentation in a 200-L bioreactor (Fig. 6b,c) and the development of a CPIII separation and purification process (Fig. 6d and Extended Data Fig. 8) have laid a solid foundation for future large-scale heme production. Based on all these data, the large-scale production processes for CPIII and heme were simulated for techno-economic analysis (Extended Data Fig. 9) to assess their industrialization potential and financial feasibility. The economic evaluation report shows that the MPSP of heme in this model is $205 per kilogram (Supplementary Table. 5). This presents a considerable cost advantage compared to the market price of heme over the last 6 years, which has ranged from $482 to $548 per kilogram (Extended Data Fig. 10b). However, the annual operating cost analysis reveals that enzymatic catalysis, including CES preparation and *E. coli* cell culture, accounts for 47% of the total heme production cost, whereas the CPIII production cost is only 34% (Extended Data Fig. 10a). This suggests that the enzymatic catalysis section accounts for most of the cost in heme production, despite the $HemQ_{28\text{-}M}$ used in this study having the highest activity ever reported. Furthermore, the results in Extended Data Fig. 7f suggest the critical need to enhance enzyme stability, alongside its activity (for example, k_{cat}). The use of HemQ enzyme with higher activity and stability can decrease enzyme dosage, eliminate the need for multiple additions of CES, streamline the process and lower heme production costs. It is noted that the MPSP of CPIII has been reduced to $67.5 per kilogram (Supplementary Table. 5). The low cost of CPIII opens up new opportunities for future scaling up the production of various other metal porphyrin compounds based on CPIIII, such as Zn-CPIII.

It is worth mentioning that this study developed two HTP screening methods for strains or enzymes. First, a genome-scale guide RNA (gRNA) library and CRISPR–dCas12a were used to develop a high-yield strain for CPIII production (Fig. 2). Additionally, this screening platform also lays a technical foundation for the further development of *R. sphaeroides* as a chassis[44]. Second, an HTP enzyme catalytic screening platform was developed using the allosteric transcription factor HrtR and CRISPR–Cas12a, along with biotin–streptavidin immobilization technology, with an operating procedure similar to the ELISA (Fig. 5a)[72]. Compared to previous methods[73], this approach is characterized by its simplicity of operation, reliable data reproducibility and robustness, which is crucial in screening highly active $HemQ_{28\text{-}M}$ for efficient production of heme by enzymatic catalysis. We think that this strategy can be expanded to facilitate HTP screening of other enzymes.

In summary, this study explores a route that combines a cell factory derived from *R. sphaeroides* with enzymatic catalysis. This strategy bypasses biological restrictions on cellular metalloporphyrin compound biosynthesis, enabling the efficient production of heme and Zn-CPIII with yields suitable for future large-scale production. Moreover, the successful pilot-scale fermentation and efficient preparation of the purified porphyrin intermediate CPIII, as well as the techno-economic analysis, suggest potential to elevate the porphyrin product manufacturing industry.

Online content

Any methods, additional references, Nature Portfolio reporting summaries, source data, extended data, supplementary information, acknowledgements, peer review information; details of author contributions and competing interests; and statements of data and code availability are available at https://doi.org/10.1038/s41587-024-02267-3.

References

1. Hiroto, S., Miyake, Y. & Shinokubo, H. Synthesis and functionalization of porphyrins through organometallic methodologies. *Chem. Rev.* **117**, 2910–3043 (2017).
2. Barr, H. et al. Eradication of high-grade dysplasia in columnar-lined (Barrett's) oesophagus by photodynamic therapy with endogenously generated protoporphyrin IX. *Lancet* **348**, 584–585 (1996).
3. Surdel, M. C. et al. Antibacterial photosensitization through activation of coproporphyrinogen oxidase. *Proc. Natl Acad. Sci. USA* **114**, E6652–E6659 (2017).
4. Drury, S. L. et al. Simultaneous exposure to intracellular and extracellular photosensitizers for the treatment of *Staphylococcus aureus* infections. *Antimicrob. Agents Chemother.* **65**, e0091921 (2021).
5. Poulos, T. L. Heme enzyme structure and function. *Chem. Rev.* **114**, 3919–3962 (2014).
6. Zhang, J. et al. Recent advances in microbial production of high-value compounds in the tetrapyrrole biosynthesis pathway. *Biotechnol. Adv.* **55**, 107904 (2022).
7. Choi, K. R., Yu, H. E., Lee, H. & Lee, S. Y. Improved production of heme using metabolically engineered *Escherichia coli*. *Biotechnol. Bioeng.* **119**, 3178–3193 (2022).
8. Zhang, W., Lai, W. & Cao, R. Energy-related small molecule activation reactions: oxygen reduction and hydrogen and oxygen evolution reactions catalyzed by porphyrin- and corrole-based systems. *Chem. Rev.* **117**, 3717–3797 (2017).
9. Singh, S. et al. Glycosylated porphyrins, phthalocyanines, and other porphyrinoids for diagnostics and therapeutics. *Chem. Rev.* **115**, 10261–10306 (2015).
10. Espinas, N. A., Kobayashi, K., Takahashi, S., Mochizuki, N. & Masuda, T. Evaluation of unbound free heme in plant cells by

differential acetone extraction. *Plant Cell Physiol.* **53**, 1344–1354 (2012).
11. In, M.-J., Kim, D. C., Chae, H. J. & Oh, N.-S. Effects of degree of hydrolysis and pH on the solubility of heme-iron enriched peptide in hemoglobin hydrolysate. *Biosci. Biotechnol. Biochem.* **67**, 365–367 (2003).
12. Lichtenthaler, H. K. & Buschmann, C. Extraction of phtosynthetic tissues: chlorophylls and carotenoids. *Curr. Protoc. Food Anal. Chem.* **1**, F4.2.1–F4.2.6 (2001).
13. Kwon Seok, J., de Boer Arjo, L., Petri, R. & Schmidt-Dannert, C. High-level production of porphyrins in metabolically engineered *Escherichia coli*: systematic extension of a pathway assembled from overexpressed genes involved in heme biosynthesis. *Appl. Environ. Microbiol.* **69**, 4875–4883 (2003).
14. Bali, S. et al. Molecular hijacking of siroheme for the synthesis of heme and d_1 heme. *Proc. Natl Acad. Sci. USA* **108**, 18260–18265 (2011).
15. Dailey Harry, A. et al. Prokaryotic heme biosynthesis: multiple pathways to a common essential product. *Microbiol. Mol. Biol. Rev.* **81**, e00048-16 (2017).
16. Dailey, H. A., Gerdes, S., Dailey, T. A., Burch, J. S. & Phillips, J. D. Noncanonical coproporphyrin-dependent bacterial heme biosynthesis pathway that does not use protoporphyrin. *Proc. Natl Acad. Sci. USA* **112**, 2210–2215 (2015).
17. Fang, H. et al. Metabolic engineering of *Escherichia coli* for de novo biosynthesis of vitamin B12. *Nat. Commun.* **9**, 4917 (2018).
18. Chen, G. E. et al. Complete enzyme set for chlorophyll biosynthesis in *Escherichia coli*. *Sci. Adv.* **4**, eaaq1407 (2018).
19. Nielsen, M. T. et al. Assembly of highly standardized gene fragments for high-level production of porphyrins in *E. coli*. *ACS Synth. Biol.* **4**, 274–282 (2015).
20. Zhang, J. et al. Heme biosensor-guided in vivo pathway optimization and directed evolution for efficient biosynthesis of heme. *Biotechnol. Biofuels Bioprod.* **16**, 33 (2023).
21. Dai, J. et al. Differential gene content and gene expression for bacterial evolution and speciation of *Shewanella* in terms of biosynthesis of heme and heme-requiring proteins. *BMC Microbiol.* **19**, 173 (2019).
22. Ouchane, S., Picaud, M., Therizols, P., Reiss-Husson, F. & Astier, C. Global regulation of photosynthesis and respiration by FnrL: the first two targets in the tetrapyrrole pathway. *J. Biol. Chem.* **282**, 7690–7699 (2007).
23. Toriya, M. et al. Zincphyrin, a novel coproporphyrin III with zinc from *Streptomyces* sp. *J. Antibiot. (Tokyo)* **46**, 196–200 (1993).
24. Nguyen, H. T. et al. Exploration of cryptic organic photosensitive compound as Zincphyrin IV in *Streptomyces venezuelae* ATCC 15439. *Appl. Microbiol. Biotechnol.* **104**, 713–724 (2020).
25. Cleary, J. L., Kolachina, S., Wolfe, B. E. & Sanchez, L. M. Coproporphyrin III produced by the bacterium *Glutamicibacter arilaitensis* binds zinc and is upregulated by fungi in cheese rinds. *mSystems*. **3**, e00036-18 (2018).
26. Zhao, X. R., Choi, K. R. & Lee, S. Y. Metabolic engineering of *Escherichia coli* for secretory production of free haem. *Nat. Catal.* **1**, 720–728 (2018).
27. Ko, Y. J. et al. Animal-free heme production for artificial meat in *Corynebacterium glutamicum* via systems metabolic and membrane engineering. *Metab. Eng.* **66**, 217–228 (2021).
28. Ishchuk, O. P. et al. Genome-scale modeling drives 70-fold improvement of intracellular heme production in *Saccharomyces cerevisiae*. *Proc. Natl Acad. Sci. USA* **119**, e2108245119 (2022).
29. Choi, K. R., Yu, H. E. & Lee, S. Y. Production of zinc protoporphyrin IX by metabolically engineered *Escherichia coli*. *Biotechnol. Bioeng.* **119**, 3319–3325 (2022).
30. Nelson, N. Metal ion transporters and homeostasis. *EMBO J.* **18**, 4361–4371 (1999).
31. Frunzke, J., Gätgens, C., Brocker, M. & Bott, M. Control of heme homeostasis in *Corynebacterium glutamicum* by the two-component system HrrSA. *J. Bacteriol.* **193**, 1212–1221 (2011).
32. Koripella, R. K. et al. Mechanism of elongation factor-G-mediated fusidic acid resistance and fitness compensation in *Staphylococcus aureus*. *J. Biol. Chem.* **287**, 30257–30267 (2012).
33. Kojima, I., Maruhashi, K., Sato, H. & Fujiwara, Y. A highly active producer of coproporphyrin III and uroporphyrin III. *J. Ferment. Bioeng.* **76**, 527–529 (1993).
34. Zhang, L. et al. Phosphate limitation increases coenzyme Q_{10} production in industrial *Rhodobacter sphaeroides* HY01. *Synth. Syst. Biotechnol.* **4**, 212–219 (2019).
35. Shi, T. et al. Screening and engineering of high-activity promoter elements through transcriptomics and red fluorescent protein visualization in *Rhodobacter sphaeroides*. *Synth. Syst. Biotechnol.* **6**, 335–342 (2021).
36. Lee, S. Q. E., Tan, T. S., Kawamukai, M. & Chen, E. S. Cellular factories for coenzyme Q_{10} production. *Microb. Cell. Fact.* **16**, 39 (2017).
37. Lu, W. et al. Identification and elimination of metabolic bottlenecks in the quinone modification pathway for enhanced coenzyme Q_{10} production in *Rhodobacter sphaeroides*. *Metab. Eng.* **29**, 208–216 (2015).
38. Wang, Z.-J. et al. Oxygen uptake rate controlling strategy balanced with oxygen supply for improving coenzyme Q_{10} production by *Rhodobacter sphaeroides*. *Biotechnol. Bioprocess Eng.* **25**, 459–469 (2020).
39. Klaus, O. et al. Engineering phototrophic bacteria for the production of terpenoids. *Curr. Opin. Biotechnol.* **77**, 102764 (2022).
40. Qiang, S. et al. Elevated β-carotene synthesis by the engineered rhodobacter sphaeroides with enhanced CrtY expression. *J. Agric. Food Chem.* **67**, 9560–9568 (2019).
41. Orsi, E. et al. Growth-uncoupled isoprenoid synthesis in *Rhodobacter sphaeroides*. *Biotechnol. Biofuels* **13**, 123 (2020).
42. Hu, J., Yang, H., Wang, X., Cao, W. & Guo, L. Strong pH dependence of hydrogen production from glucose by *Rhodobacter sphaeroides*.*Int. J. Hydrog. Energy* **45**, 9451–9458 (2020).
43. Li, S. et al. Photoautotrophic hydrogen production of *Rhodobacter sphaeroides* in a microbial electrosynthesis cell. *Bioresour. Technol.* **320**, 124333 (2021).
44. Orsi, E., Beekwilder, J., Eggink, G., Kengen, S. W. M. & Weusthuis, R. A. The transition of *Rhodobacter sphaeroides* into a microbial cell factory. *Biotechnol. Bioeng.* **118**, 531–541 (2021).
45. Oh, J.-I. & Kaplan, S. Generalized approach to the regulation and integration of gene expression. *Mol. Microbiol.* **39**, 1116–1123 (2001).
46. Imam, S., Noguera, D. R. & Donohue, T. J. Global analysis of photosynthesis transcriptional regulatory networks. *PLoS Genet.* **10**, e1004837 (2014).
47. Kang, Z. et al. Recent advances in microbial production of δ-aminolevulinic acid and vitamin B12. *Biotechnol. Adv.* **30**, 1533–1542 (2012).
48. Nishikawa, S. et al. *Rhodobacter sphaeroides* mutants which accumulate 5-aminolevulinic acid under aerobic and dark conditions. *J. Biosci. Bioeng.* **87**, 798–804 (1999).
49. Urakami, T. & Yoshida, T. Production of ubiquinone and bacteriochlorophyll *a* by *Rhodobacter sphaeroides* and *Rhodobacter sulfidophilus*. *J. Ferment. Bioeng.* **76**, 191–194 (1993).
50. Zeilstra-Ryalls, J. H. & Kaplan, S. Aerobic and anaerobic regulation in *Rhodobacter sphaeroides* 2.4.1: the role of the *fnrL* gene. *J. Bacteriol.* **177**, 6422–6431 (1995).
51. Wei, W. et al. Lysine acetylation regulates the function of the global anaerobic transcription factor FnrL in *Rhodobacter sphaeroides*. *Mol. Microbiol.* **104**, 278–293 (2017).

52. Tao, Y. et al. Characteristics of a new photosynthetic bacterial strain for hydrogen production and its application in wastewater treatment. *Int. J. Hydrog. Energy* **33**, 963–973 (2008).
53. Qu, Y., Su, A., Li, Y., Meng, Y. & Chen, Z. Manipulation of the regulatory genes *ppsR* and *prrA* in *Rhodobacter sphaeroides* enhances lycopene production. *J. Agric. Food Chem.* **69**, 4134–4143 (2021).
54. Rowan-Nash Aislinn, D., Korry Benjamin, J., Mylonakis, E. & Belenky, P. Cross-domain and viral interactions in the microbiome. *Microbiol. Mol. Biol. Rev.* **83**, e00044-00018 (2019).
55. Dailey, T. A. et al. Discovery and characterization of HemQ: an essential heme biosynthetic pathway component. *J. Biol. Chem.* **285**, 25978–25986 (2010).
56. Toriya, M., Yamamoto, M., Saeki, K., Fujii, Y. & Matsumoto, K. Antitumor effect of photodynamic therapy with zincphyrin, zinc-coproporphyrin III, in mice. *Biosci. Biotechnol. Biochem.* **65**, 363–370 (2001).
57. Yamamoto, M. et al. Production of singlet oxygen on irradiation of a photodynamic therapy agent, zinc-coproporphyrin III, with low host toxicity. *Biometals* **16**, 591–597 (2003).
58. Voigt, C. A. Synthetic biology 2020–2030: six commercially-available products that are changing our world. *Nat. Commun.* **11**, 6379 (2020).
59. Lechardeur, D. et al. Discovery of intracellular heme-binding protein HrtR, which controls heme efflux by the conserved HrtB-HrtA transporter in *Lactococcus lactis*. *J. Biol. Chem.* **287**, 4752–4758 (2012).
60. Zou, Z.-P., Du, Y., Fang, T.-T., Zhou, Y. & Ye, B.-C. Biomarker-responsive engineered probiotic diagnoses, records, and ameliorates inflammatory bowel disease in mice. *Cell Host Microbe* **31**, 199–212 (2023).
61. Weber, P. C., Ohlendorf, D. H., Wendoloski, J. J. & Salemme, F. R. Structural origins of high-affinity biotin binding to streptavidin. *Science* **243**, 85–88 (1989).
62. Chen, J. S. et al. CRISPR–Cas12a target binding unleashes indiscriminate single-stranded DNase activity. *Science* **360**, 436–439 (2018).
63. Celis, A. I. et al. Structure-based mechanism for oxidative decarboxylation reactions mediated by amino acids and heme propionates in coproheme decarboxylase (HemQ). *J. Am. Chem. Soc.* **139**, 1900–1911 (2017).
64. Griffiths, M. & Stanier, R. Y. Some mutational changes in the photosynthetic pigment system of *Rhodopseudomonas spheroides*. *Microbiology* **14**, 698–715 (1956).
65. Skotnicová, P. et al. The cyanobacterial protoporphyrinogen oxidase HemJ is a new *b*-type heme protein functionally coupled with coproporphyrinogen III oxidase. *J. Biol. Chem.* **293**, 12394–12404 (2018).
66. Kanazireva, E. & Biel, A. J. Cloning and overexpression of the *Rhodobacter capsulatus* hemH gene. *J. Bacteriol.* **177**, 6693–6694 (1995).
67. Yoshida, H., Kotani, Y., Ochiai, K. & Araki, K. Production of ubiquinone-10 using bacteria. *J. Gen. Appl. Microbiol.* **44**, 19–26 (1998).
68. Gibson, L. C. D., McGlynn, P., Chaudhri, M. & Hunter, C. N. A putative anaerobic coproporphyrinogen III oxidase in *Rhodobacter sphaeroides*. II. Analysis of a region of the genome encoding *hemF* and the *puc* operon. *Mol. Microbiol.* **6**, 3171–3186 (1992).
69. Oh, J.-I., Eraso Jesus, M. & Kaplan, S. Interacting regulatory circuits involved in orderly control of photosynthesis gene expression in *Rhodobacter sphaeroides* 2.4.1. *J. Bacteriol.* **182**, 3081–3087 (2000).
70. Eraso, J. M. & Kaplan, S. *prrA*, a putative response regulator involved in oxygen regulation of photosynthesis gene expression in *Rhodobacter sphaeroides*. *J. Bacteriol.* **176**, 32–43 (1994).
71. Oh, J.-I., Ko, I.-J. & Kaplan, S. The default state of the membrane-localized histidine kinase Prrb of *Rhodobacter sphaeroides* 2.4.1 is in the kinase-positive mode. *J. Bacteriol.* **183**, 6807–6814 (2001).
72. Hornbeck, P. V. Enzyme-linked immunosorbent assays. *Curr. Opin. Immunol.* **110**, 2.1.1–2.1.23 (2015).
73. Liang, M. et al. A CRISPR–Cas12a-derived biosensing platform for the highly sensitive detection of diverse small molecules. *Nat. Commun.* **10**, 3672 (2019).

Publisher's note Springer Nature remains neutral with regard to jurisdictional claims in published maps and institutional affiliations.

Springer Nature or its licensor (e.g. a society or other partner) holds exclusive rights to this article under a publishing agreement with the author(s) or other rightsholder(s); author self-archiving of the accepted manuscript version of this article is solely governed by the terms of such publishing agreement and applicable law.

© The Author(s), under exclusive licence to Springer Nature America, Inc. 2024

Methods

Strains, plasmids and culture conditions

The plasmids and strains used in this study are listed in Supplementary Tables 6 and 7. *E. coli* DH10b, *E. coli* BL21(DE3), *E. coli* S17-1 and their derivatives were cultivated on Luria–Bertani (LB) agar plates (tryptone 10 g L^{-1}, yeast extract 5 g L^{-1} and NaCl 10 g L^{-1}, pH 7.0) at 37 °C. *R. sphaeroides* and its derivatives were cultivated on agar plates (0.3% glucose, 0.8% yeast extract, 0.13% monobasic potassium phosphate, 0.2% sodium chloride, 0.0125% magnesium sulfate and 1.5% agar, supplemented with 15 mg L^{-1} biotin, 1 mg L^{-1} thiamine hydrochloride and 1 mg L^{-1} nicotinic acid). For CPIII fermentation in a 250-ml shake flask or a 5-L bioreactor, *R. sphaeroides* and its derivatives were cultivated in seed medium (per liter of medium includes: 1.5% glucose, 0.2% yeast extract, 0.1% sodium glutamate, 0.1% corn steep liquor, 0.4% $(NH_4)_2SO_4$, 0.1% KH_2PO_4, 0.1% K_2HPO_4, 0.02% $FeSO_4$, 0.36% $MgSO_4$, 0.2% NaCl, 2 ml of 10 g L^{-1} manganese sulfate solution and 1.5 ml of 10 g L^{-1} cobalt chloride solution, pH 7.1–7.2.) and fermentation medium (4% glucose, 0.4% corn steep liquor, 0.3% sodium glutamate, 0.3% $(NH_4)_2SO_4$, 0.28% NaCl, 0.3% KH_2PO_4, 0.63% $MgSO_4$ and 0.2% $CaCO_3$ supplemented with 1 mg L^{-1} thiamine hydrochloride, 1 mg L^{-1} nicotinic acid and 15 μg L^{-1} biotin). All the reagents and chemicals used for culture media were provided by Titan Scientific Co., Ltd.

Genetic manipulation in *R. sphaeroides*

The primers used for plasmids construction are listed in Supplementary Table. 8. For *fnrL* and *hemN* gene deletion or $prrAB_{pLB2}$ gene replacement in *R. sphaeroides*, plasmid pK18mobsacB (pK18mob) was digested by *Hind*III (New England Biolabs (NEB), R3104) and *EcoR*I (NEB, R3101) to obtain a linear vector, and a high-fidelity GXL polymerase (TaKaRa Bio, R050A) was used to amplify two 500–1,000-bp homology arms by using *R. sphaeroides* genomic DNA as template. The linear vector DNA and PCR products were assembled with a NovoRec plus One step PCR Cloning Kit (Novoprotein, NR005). The plasmid was introduced into *R. sphaeroides* with the help of *E. coli* S17-1 by intergeneric conjugation, and exconjugants with single crossover were selected for kanamycin resistance (kan^R). Then, the mutant was selected from the initial exconjugants after several rounds of non-selective growth and confirmed by PCR amplification using the primers listed in Supplementary Table 10. The DNA gel images were captured with a Tanon 1600 Gel Image System (Tanon Biotech).

CRISPRi and genome-wide transformant screening

A codon-optimized dCas12a coding gene (based on *R. sphaeroides*) was synthesized and cloned into the pBBR-Prsp_7571-gusA plasmid[35] by replacing *gusA* gene, resulting pBBR-Prsp_7571-dcas12a plasmid. Another cassette containing the P_{rsp_7571} promoter[35], *Sap*I restriction site and a *puf* operon-specific transcription terminator was synthesized and then cloned into pBBR-Prsp_7571-dcas12a, resulting pBBR-dCas12a plasmid. For CRISPRi, the oligonucleotides encoding crRNA (Supplementary Table 9) were cloned into pBBR-dCas12a plasmid by using *Sap*I (NEB, R0569S). Based on the previously reported protocol[74], the crRNAs used for detecting CRISPRi efficiency were synthesized in vitro using a HiScribe T7 Quick High Yield RNA Synthesis Kit (NEB, E2040S). For CRISPRi-based transformants screening, a genome-wide crRNA library of *R. sphaeroides* containing 12,820 crRNAs was designed by Python programming (software version 3.8; Supplementary Note 1) and synthesized. The corresponding plasmid library was obtained by introducing the crRNA library into pBBR-dCas12a plasmid. After introducing the plasmid (or plasmid library) into *R. sphaeroides* via the optimized conjugation method (Supplementary Note 4), the corresponding transformants can be screened based on their resistance or color phenotype. The oligonucleotides, genes, crRNA library and plasmid library were synthesized and assembled by GenScript.

Fed-batch fermentation in a 5-L bioreactor and sampling

Fed-batch fermentation of CPIII was performed in a 5-L stirred bioreactor (Shanghai Bailun Biotechnology Co., Ltd., BLBIO-5GJ-3) with an initial working volume of 2.5 L. Dissolved oxygen (DO) and pH were measured by a DO probe (Hamilton, VisiFerm DO Arc 225 H2) and a pH electrode (Hamilton, EasyFerm Plus PHI Arc 225), respectively. Foam formation was prevented by the addition of antifoam 204 (Sigma-Aldrich). The temperature was maintained at a constant 32 °C, aeration at 1.0 air volume/culture volume/min (VVM), agitation at 600 r.p.m. and pH at 6.5 by automatic injection of ammonia. The fed-batch process was initiated after 18 h of cultivation, using a concentrated glucose stock solution of 500 g L^{-1} to maintain a glucose concentration of 15 g L^{-1} in the bioreactor. After 48 h, the glucose concentration was maintained at 5 g L^{-1}, with a 25-ml supplementation of feeding medium (glucose-free fermentation medium) every 24 h. Fermentation broth was collected every 6 h during the fermentation process for monitoring cell growth (OD_{700}) and the titer of CPIII.

HPLC detection of porphyrin compounds

CPIII, heme and other metalloporphyrins involved in this study were analyzed using HPLC. Then, 200 μl of the sample (for example, fermentation broth supernatant or enzyme-catalyzed reaction solution) was mixed with an equal volume of 0.05% acidic acetone, shaken vigorously and centrifuged at 13,800*g* for 1 min (Thermo Fisher Scientific, 37520). The resulting supernatant was then filtered through a 0.22-μm membrane into a brown sample vial for subsequent HPLC detection. Standard stock solutions of CPIII (Macklin, C882263), Fe-CPIII (Frontier Scientific, C40019) and heme (Sigma-Aldrich, 51280) were respectively prepared at a concentration of 1 mg ml^{-1} for quantitative analysis. An Agilent 1100 series HPLC system equipped with an InfinityLab Poroshell 120 EC-C18 column (4 μm, 4.6 × 150 mm, Agilent) and a multiple wavelength detector (DAD) was used for detection. The mobile phase consisted of a gradient elution with 0.1% formic acid in water (phase A) and methanol (phase B), flowing at a rate of 1 ml min^{-1}. The detection wavelength was set at 390 nm. HPLC data were collected using Agilent OpenLAB CDS ChemStation Edition for LC and LC–MS systems (version C.01.07 SR2 (255)). Agilent OpenLAB CDS ChemStation Editor (version C.01.10 (201)) was used for data analysis.

Mass spectrometry detection of porphyrin compounds

The enzyme reaction solution (or fermentation broth supernatant) containing target porphyrin compounds was mixed with an equal volume of 0.05% acidic acetone, shaken vigorously and centrifuged at 13,800*g* for 10 min. The supernatant was collected, and an appropriate amount of the sample was mixed with methanol to achieve a sample concentration below 0.5 mg ml^{-1}. After filtering through a 0.22-μm membrane, the sample was analyzed using a Thermal UltiMate 3000 UHPLC coupled with a Q Exactive Orbitrap mass spectrometer (Thermo Fisher Scientific) equipped with a positive ESI source. A Waters ACQUITY BEH C18 chromatographic column (150 mm × 4.6 mm, 1.7 μm particle size) was used with a mobile phase of 0.1% formic acid in water and methanol, at a flow rate of 0.35 ml min^{-1}. Full-scan mass spectrometry was performed in the range of 100–1,200 Da (resolution: 70,000, scan time: 50 ms). The mass spectrometry data were analyzed using Xcalibur Qual Browser (software version 3.1, Thermo Fisher Scientific).

Pilot-scale fermentation of CPIII in a 200-L bioreactor

Single colonies of *R. sphaeroides* HY01-Δ$hemN$-$prrAB_{pLB2}$ were selected from agar plates and inoculated into a 500-ml shake flask containing 50 ml of seed culture medium. The cultures were incubated at 32 °C with agitation at 220 r.p.m. in the dark for 25–28 h. Subsequently, a 1% inoculum of the primary seed culture was transferred into 2-L shake flasks containing 250 ml of seed culture medium. The resulting secondary cultures were incubated at 32 °C with agitation at 220 r.p.m. for 23–26 h. After this, a 10% inoculum of the secondary seed culture was transferred into a 20-L bioreactor containing 15 L of seed culture. The fermentation conditions included pressure of 0.03 MPa, temperature at 32 °C, agitation at 420 r.p.m. and aeration at 1 vvm (volumes of air per liquid

volume per minute) for 16–20 h. Finally, a 20% inoculum of the resulting tertiary seed culture was introduced into a 200-L bioreactor (Baoxing Co., Ltd., BIOTECH-3000) containing 75 L of fermentation medium. The fermentation conditions maintained pressure of 0.03–0.04 MPa, agitation at 300–350 r.p.m. and aeration at 1–2 vvm. Throughout the fermentation process, pH was stabilized around 6.5 using ammonia solution. Simultaneously, the glucose concentration was kept between 5 g L^{-1} and 8 g L^{-1}. IPTG was added into the bioreactor at approximately 30 h of fermentation (with final concentration of 1 mM). Feeding was performed every 24 h, and samples were taken every 4–6 h to measure cell density, residual sugar and CPIII production.

Purification and preparation of CPIII by crystallization

The fermentation broth was centrifuged at 6,869*g* for 5 min (Thermo Fisher Scientific, Sorvall RC-5B Plus Superspeed Centrifuge) to collect the supernatant. The pH of the supernatant was adjusted to 8.5 using NaOH and left to stand in the dark at room temperature for 30 min. Subsequently, the supernatant was collected by centrifugation (6,869*g* for 5 min). Later, 20% isopropanol was added and thoroughly mixed, followed by incubation in the dark at room temperature for 2 h. The solution was then centrifuged at 6,869*g* for 5 min to collect the supernatant. Subsequently, 30% volume of acidic acetone was added, stirred thoroughly and centrifuged to remove precipitates, obtaining the remaining solution. In the resulting remaining solution, 1% sodium acetate was added, and the mixture was left to stand in the dark at low temperature for 16 h. The supernatant was discarded after centrifugation, and the collected CPIII crystals were dried. For recrystallization, dried CPIII crystals were completely dissolved in 0.1 M NaOH and centrifuged at 6,869*g* for 5 min, and the supernatant was collected. Then, the pH of the resulting supernatant was adjusted to 4.5 using acetic acid, and the crystals were collected by centrifugation, washed with deionized water and dried to obtain crystals. To determine the purity of CPIII crystal samples, the samples were weighed and dissolved in DMSO to prepare a 10 mg L^{-1} solution. The peak area (f1) of the sample was measured by HPLC. Subsequently, a solution with the same concentration of CPIII standard was prepared, and its peak area (f2) was measured by HPLC. This experiment was repeated three times, and the purity was calculated based on the comparison of the peak areas of the sample, using equation 1, where p represents the purity of the standard sample (%). The weight of dried CPIII crystals (m) was measured, and the recovery rate was calculated using equation 2, where m is the total weight of the obtained CPIII crystals (g), and purity (%) is calculated using equation 1. The concentration of CPIII in the fermentation broth (g L^{-1}) is represented by C, and the volume of the fermentation broth is represented by V (L).

$$Purity(\%) = \frac{f1}{f2 * p} \times 100\% \quad (1)$$

$$Recovery\ rate(\%) = \frac{\text{Purity}(\%) \cdot m}{C \cdot V} \quad (2)$$

Biosynthesis of metalloporphyrins using CPIII

$FeSO_4{\cdot}7H_2O$, $FeCl_3{\cdot}6H_2O$, $CoCl_2{\cdot}6H_2O$, $NiSO_4{\cdot}6H_2O$, $CuCl_2{\cdot}2H_2O$, $MgSO_4{\cdot}7H_2O$ and $ZnCl_2$ were dissolved in deionized water to prepare stock solutions of different metal ions at a concentration of 5 mM each. All of these metal salts were purchased from Sangon Biotech Co. Ltd. Subsequently, in a Tris-HCl buffer (50 mM, pH 7.0), 50 μM of CPIII and 50 μM of each metal ion salt solution was added and mixed thoroughly. Finally, 1 μM of HemH enzyme was added to initiate the reaction. Unless otherwise specified, this experiment was typically conducted at 37 °C for 30 min. Under the same reaction conditions, a control experiment was also conducted without the addition of HemH enzyme to investigate the spontaneous reaction of CPIII with different metal ions. After the reaction was completed, an equal volume of acidic acetone (containing 2% HCl) was added and mixed by vortex oscillation. The solution was then centrifuged at 16,200*g* for 3 min. The supernatant was filtered through a 0.22-μm filter, and the formation of metal porphyrin compounds was analyzed using HPLC and high-resolution mass spectrometry.

Proteins overexpression and preparation of CES

The proteins used for in vitro enzymatic catalysis were overexpressed in pET28a in *E. coli* BL21 (DE3). Single clones were selected from LB agar plates and inoculated into 10 ml of LB medium containing 0.1% kanamycin. The cultures were incubated overnight at 37 °C with shaking at 200 r.p.m. Subsequently, a 1% volume transfer was performed to scale up the culture. When the OD_{600} reached 0.6–0.8, the culture was induced with IPTG (Sigma-Aldrich, I6758) at a final concentration of 0.1 mmol L^{-1} and incubated at a low temperature (16 °C) for 16–18 h. The cells were then harvested by centrifugation at 3,864*g* for 5 min and weighed. The cell pellet was resuspended in an appropriate buffer (50 mM Tris-HCl) and mixed thoroughly. Sonication in an ice bath (40 cycles of 3-s sonication with a 10-s interval) was used to achieve cell disruption on a small scale (Ningbo Scientz Biotechnology Co., Ltd.). For large-scale cell disruption, a high-pressure treatment using a cell disruptor (JNBIO) was employed. The resulting cell lysate was centrifuged at 13,300*g* for 45 min at 4 °C. The supernatant was collected, and protein expression was confirmed by SDS-PAGE. For preparation of CES, once the enzyme activity meets the required criteria, the lysate supernatant can be used as CES for subsequent enzyme catalysis experiments. For protein purification, the supernatant of the cell lysate was loaded onto a HisTrap FF column (GE Healthcare) and washed with a gradient of imidazole concentrations. The fractions containing the desired protein peak were collected and subjected to desalting through dialysis. The fractions were further analyzed using SDS-PAGE, and their concentrations were determined using the Bradford method.

Enzyme activity, K_m and k_{cat} determination

In this study, enzyme activity unit (U) was defined as the amount of enzyme required to catalyze the conversion of 1 μM substrate or generate 1 μM product within 1 min under optimal temperature (37 °C) and pH conditions. In the range of substrate concentrations from 0 μM to 100 μM, the enzymatic reaction kinetics parameters of HemQ on the substrate Fe-CPIII are determined. First, in the reaction system (50 mM Tris HCl, pH 7.0), 0.5 μM hydrogen peroxide and different concentrations of Fe-CPIII were added. Then, a final concentration of 24 μM purified HemQ enzyme was added, and the reaction was carried out at 37 °C for various timepoints. After the reaction was complete, an equal volume of 4% hydrochloric acid and acetone solution (prepared fresh) was added, followed by vortexing and centrifugation at 13,300*g* for 10 min to collect the supernatant. The concentration of substrate and product was determined by filtering through a 0.22-μm membrane and analyzing peak areas using HPLC. The Michaelis–Menten equation was fitted to the data using GraphPad Prism (version 9.5.1, GraphPad Software), and the K_m and k_{cat} values were obtained through the curve fitting process.

Biotinylation of HrtR and gel shift assay

The *hrtR* gene, derived from *L. lactis*[59], was codon optimized and expressed in *E. coli* to produce the protein. Then, 500 μl of 80 μM HrtR protein was incubated on ice for 2 h with the addition of 50 μl of a 10 mM sulfosuccinimidobiotin solution (Sangon Biotech Co., Ltd.), resulting in Biot-HrtR protein. The resulting 550 μl of reaction mixture was adjusted to a final volume of 2.5 ml with PBS buffer and thoroughly mixed. Subsequently, the mixture was loaded onto a pre-equilibrated desalting column (Cytiva, 17085101) with PBS buffer, and the eluted fractions were collected. The concentration of Biot-HrtR protein was determined using a BCA protein quantification assay (Beyotime Biotechnology). The concentration was

adjusted to 8 μM with PBS and stored at −80 °C in 10% glycerol for future use. The conformational activity of Biot-HrtR was validated using EMSA. Initially, a 33-bp dsDNA probe was generated by annealing two oligos (5′-TAGAATTTAATAAATGACACAGTGTCATAAATT-3′ and 5′-AATTTATGACACTGTGTCATTTATTA-AATTCTA-3′) and employed as the probe for the EMSA experiment. The probe was incubated at room temperature for 30 min with different concentrations (0 nM, 31 nM, 62 nM, 125 nM and 250 nM) of Biot-HrtR protein in 20 μl of binding buffer (10 mM Tris-HCl (pH 7.5), 100 mM KCl, 1 mM EDTA, 0.1 mM DTT, 5% v/v glycerol, 0.01 mg ml^{-1} BSA)[73]. For the dissociation assays, different concentrations of heme or other structural analogs, such as coproporphyrin I (Sigma-Aldrich, 258784), CPIII, Fe-CPIII and protoporphyrin (Sigma-Aldrich, P8293), were added to the binding reaction mixtures. After incubation, the mixtures were separated in 1.5% agarose gel with Tris-borate-EDTA buffer at 4 °C. The band shifts were detected and analyzed with a ChemiDoc XRS+ Imaging System (Bio-Rad).

Heme sensing and HTP enzyme screening

The plasmid library of HemQ variants was introduced into $CaCl_2$-treated *E. coli* BL21(DE3) through the heat shock method. The transformed cells were spread on LB agar plates containing kanamycin and incubated overnight to obtain single colonies. Individual colonies were picked and cultured in 96-well plates containing LB medium until the OD_{600} reached between 0.4 and 0.8. After preserving backup cultures, the cultivation temperature was lowered from 37 °C to 16 °C. After 48 h of induction and protein expression, the cells were then harvested by centrifugation, and the culture medium was discarded. Next, 200 μl of lysozyme solution (containing 2 g L^{-1} lysozyme and 0.1% Triton X-100 in PBS, pH 7.0) was added to each well to lyse the cells. Subsequently, 10 μl of reaction mixture (containing 5 μM Fe-CPIII) was added to each well, followed by incubation at 37 °C for 40 min. After that, 200 μl of 2% acid-acetone solution was added and mixed, and then 400 μl of PBS buffer was added and mixed. Next, 50 μl of the reaction mixture was taken and added to a 96-well plate coated with streptavidin-linked HrtR (where Biot-HrtR was already saturated with dsDNA), and the reaction was allowed to proceed for 10 min. Then, 10 μl of the reaction mixture was added to a fluorescence colorimetric system containing CRISPR–Cas12a and FQ-labeled probe[73]. Finally, the signals were read using a fluorescence microplate reader (software version 5.20 R5, BMG CLARIOstar, BMG LABTECH) at an excitation wavelength of 480 nm and an emission wavelength of 520 nm. Analyzing the fluorescence intensity by MARS Data Analysis Software (version 3.20. R2, BMG LABTECH) can help screen for highly active HemQ mutants (Extended Data Fig. 6).

Scale-up enzymatic synthesis of heme and Zn-CPIII

For the enzymatic synthesis of heme in a 5-L bioreactor, initially, 180 g of *E. coli* cells expressing the $HemH_{Sa}$ and $HemQ_{28\text{-}M}$ fusion protein was used. These cells were then suspended in 500 ml of Tris-HCl buffer (pH 7.0) to ensure complete resuspension. Subsequently, the cells were subjected to two rounds of cell disruption using a high-pressure homogenizer (JNBIO), followed by centrifugation at 4 °C and 15,455*g* for 25 min to collect the CES. A total of 38 g of CPIII sample prepared through fermentation and recrystallization (purity 95.2%) was dissolved in 100 ml of DMSO. Simultaneously, 153 g of $FeSO_4{\cdot}7H_2O$ was dissolved in 100 ml of 50 mM Tris-HCl (pH 7) to prepare the $FeSO_4{\cdot}7H_2O$ stock solution. In the 5-L bioreactor, 1,100 ml of 50 mM Tris-HCl (pH 7) solution was added, along with 100 ml of the prepared CPIII solution and the required amount of $FeSO_4{\cdot}7H_2O$ solution. The temperature was maintained at 37 °C with agitation at 50 r.p.m. The reaction was initiated after the first addition of the CES, and subsequent additions were made at different timepoints based on optimized conditions. Samples were taken every 2 h to measure the concentrations of the substrate CPIII, the intermediate product Fe-CPIII and the final product Heme. The reaction was concluded when heme production ceased. For the enzymatic synthesis of Zn-CPIII, 30 g of *E. coli* cells expressing $HemH_{Sa}$ was prepared. After being resuspended in 150 ml of Tris-HCl (pH 7.0), $HemH_{Sa}$ enzyme solution was collected by centrifugation (4 °C, 15,455*g*, 25 min) following cell disruption using a high-pressure homogenizer (JNBIO). Another 21 g of CPIII sample, prepared through fermentation and recrystallization (purity 95.2%), was dissolved in DMSO and added to a 5-L bioreactor containing 0.9 L of 50 mM Tris-HCl (pH 7.0). Then, 4.5 g of $ZnCl_2$, dissolved in 50 mM Tris-HCl (pH 7.0), was added to the bioreactor, and the temperature was maintained at 37 °C with agitation at 50 r.p.m. The reaction was initiated with a one-time addition of the crude $HemH_{Sa}$ enzyme solution, and subsequent samples were taken to monitor the conversion of CPIII and the generation of Zn-CPIII.

Techno-economic analysis of CPIII and heme production

SuperPro Designer version 10.7 simulation software (Intelligen) was used to construct techno-economic analysis. A model for an industrial installation aimed at the commercial production of CPIII and heme was developed based on data from 200-L pilot-scale fed-batch CPIII fermentation (Fig. 6c) and subsequent CPIII preparation (Extended Data Fig. 8) as well as data on heme production through enzymatic catalysis in a 5-L bioreactor (Fig. 6e,f), using software simulation. The feasibility of the process is demonstrated by analyzing the annual operating costs, which mainly include raw materials, labor costs, consumables, utilities, equipment costs (maintenance, depreciation and miscellaneous costs) and waste disposal costs. Raw material prices are shown in Supplementary Table. 4. The MPSP was estimated in 2024 dollars. The costs and prices of water, steam, electricity, wastewater treatment and waste solids disposal benefit from policies provided by Tuoketuo Power Industrial Park in Hohhot, China. Detailed information was provided by the local investment promotion department.

Data analysis

Data analysis and process were carried out using Microsoft Excel 2016. If not specified otherwise, the data in the figures are presented as the mean ± s.d. Where relevant, two-tailed Student's *t*-tests were used to demonstrate differences in values. $P < 0.05$ was used as a standard criterion of statistical significance. Chemical compounds displayed in this paper were produced by CambridgeSoft ChemBioDraw Ultra (version 12.00). Bar charts (overlapped with their corresponding data points) were plotted using GraphPad Prism 9 software.

Reporting summary

Further information on research design is available in the Nature Portfolio Reporting Summary linked to this article.

Data availability

The authors declare that the primary data supporting the findings of this study are accessible within the paper and its Supplementary Information files. Additional data can be obtained from the corresponding author upon reasonable request. Source data are provided with this paper.

Code availability

The developed code in this work is available at https://codeocean.com/capsule/8302979/tree/v1 or https://doi.org/10.24433/CO.8752603.v1.

References

74. Zeng, X. et al. An in vitro CRISPR–Cas12a-mediated protocol for direct cloning of large DNA fragments. *STAR Protoc.* **4**, 102435 (2023).

Acknowledgements

We thank Q. Chen (School of Biotechnology, East China University of Science and Technology), L. Zhang (School of Chemistry and Molecular Engineering, East China Normal University) and W. Zhang (State Key Laboratory of Microbial Technology, Shandong University) for their

technical support in enzyme mining, engineering and characterization. We are also deeply grateful to Z. Zhou (Institute of Plant Physiology and Ecology, Chinese Academy of Sciences) for her generous gift of the ZX-5 strain and to Inner Mongolia Kingdomway Pharmaceutical Co., Ltd. for providing the HY01 strain. We would like to extend our gratitude to D.-Q. Lin from the College of Chemical and Biological Engineering at Zhejiang University for his invaluable guidance in conducting the techno-economic analysis and for providing assistance in using the SuperPro Designer simulation software. During the manuscript preparation, we also greatly appreciate the constructive insights provided by J.-J. Zhong, L. Bai and T. Liu from the School of Life Sciences and Biotechnology, Shanghai Jiao Tong University. This work was financially supported, in part, by grants from the National Key Research and Development Program of China (2020YFA0907800 to Z.L. and 2020YFA0907304 to T.G.-Y.); the National Natural Science Foundation of China (32370064 and 31870040 to T.G.-Y.); 2023 Double World-Class Project-Key Program-Intelligent Biomanufacturing to Z.L.; and the Open Funding Project of the State Key Laboratory of Microbial Metabolism (MMLKF22-03 to T.G.-Y.).

Author contributions

G.-Y.T. and Lixin Zhang supervised the project. G.-Y.T., Lixin Zhang and W.W. designed the experiments. Lu Zhang, T.S., X.H., M.Y., W.J. and D.L. engineered and optimized *R. sphaeroides*. Z.W. and H.C. designed the crRNA library and screened the strains. T.C., X.C., H.C., Z.W., X.W. and B.G. mined the enzyme and performed enzymatic catalysis. Y.W., X.C. and M.L. developed the heme detection method and conducted high-throughput screening work. H.W., H.C., G.Z., X.L., J.Z., H.L., X.X. and Y.X. isolated, prepared and identified chemical compounds. H.C., Z.W., L.O., Y.L., J.Y. and Z.L. conducted the fed-batch work in bioreactor. H.C., Z.W. and Z.L. developed the pilot-scale fermentation process and the method for isolating and purifying CPIII. Z.W. and H.C. conducted the techno-economic analysis. G.-Y.T. wrote the manuscript. Lixin Zhang, G.-Y.T. and Y.T. edited the manuscript.

Competing interests

G.-Y.T, Lixin Zhang, W.W., Lu Zhang, Y.W., T.C. and H.C. filed eight Chinese patent applications (201910999107.4, 202211452809.9, 202211487904.2, 202310737429.8, 202310738915.1, 202310750263.3, 202310754364.8 and 2023118130742) based on this work. The remaining authors declare no competing interests.

Additional information

Extended data is available for this paper at https://doi.org/10.1038/s41587-024-02267-3.

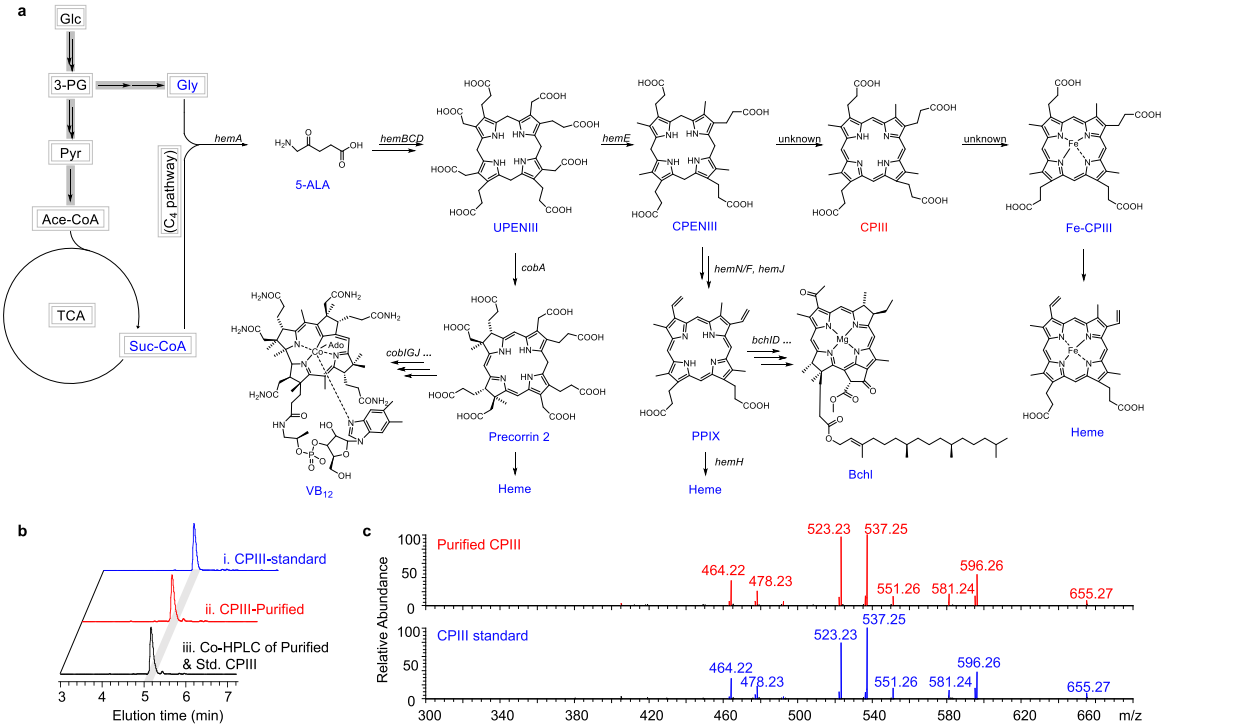
Supplementary information The online version contains supplementary material available at https://doi.org/10.1038/s41587-024-02267-3.

Correspondence and requests for materials should be addressed to Gao-Yi Tan or Lixin Zhang.

Peer review information *Nature Biotechnology* thanks the anonymous reviewers for their contribution to the peer review of this work.

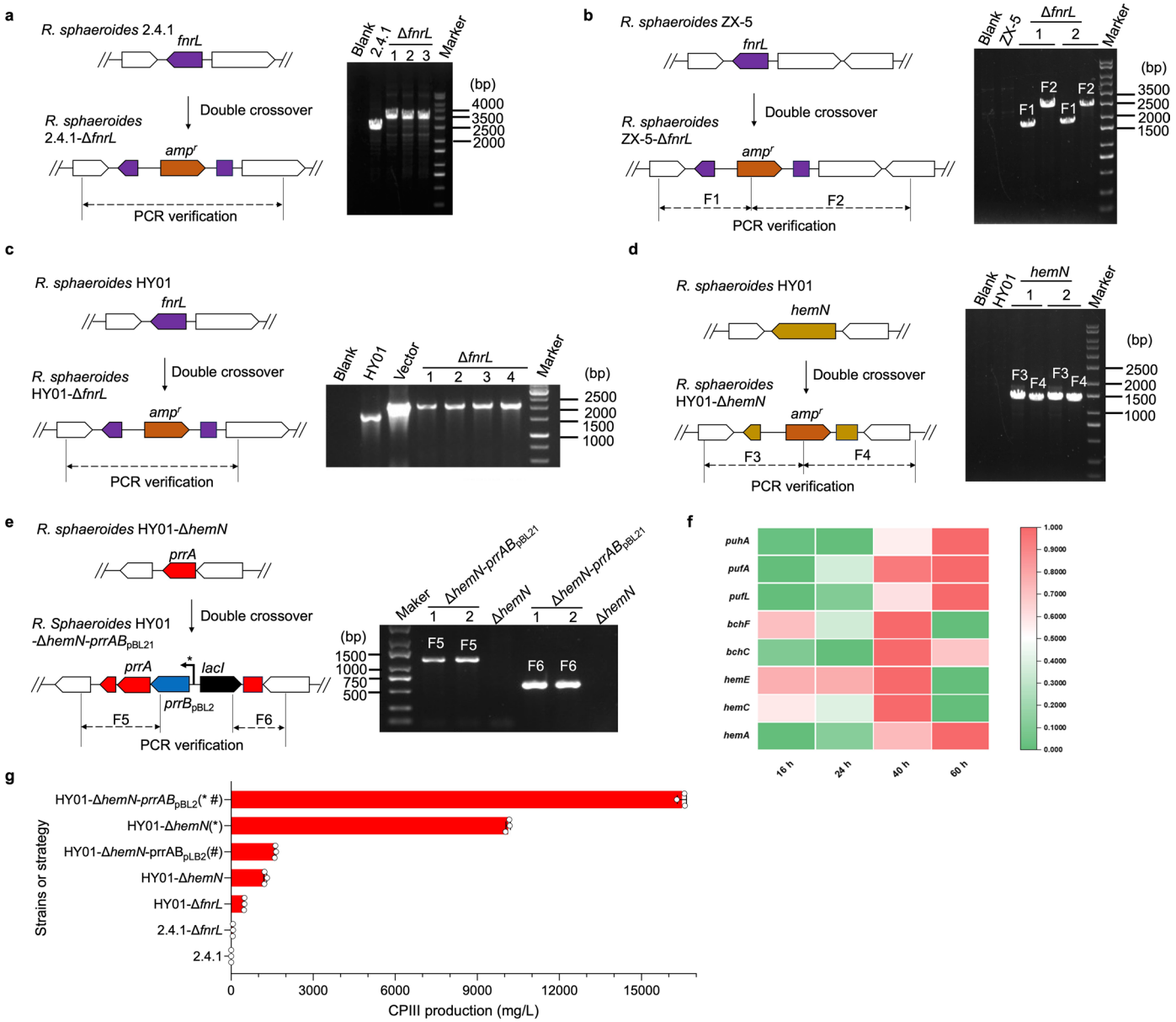
Reprints and permissions information is available at www.nature.com/reprints.

https://doi.org/10.1038/s41587-024-02267-3



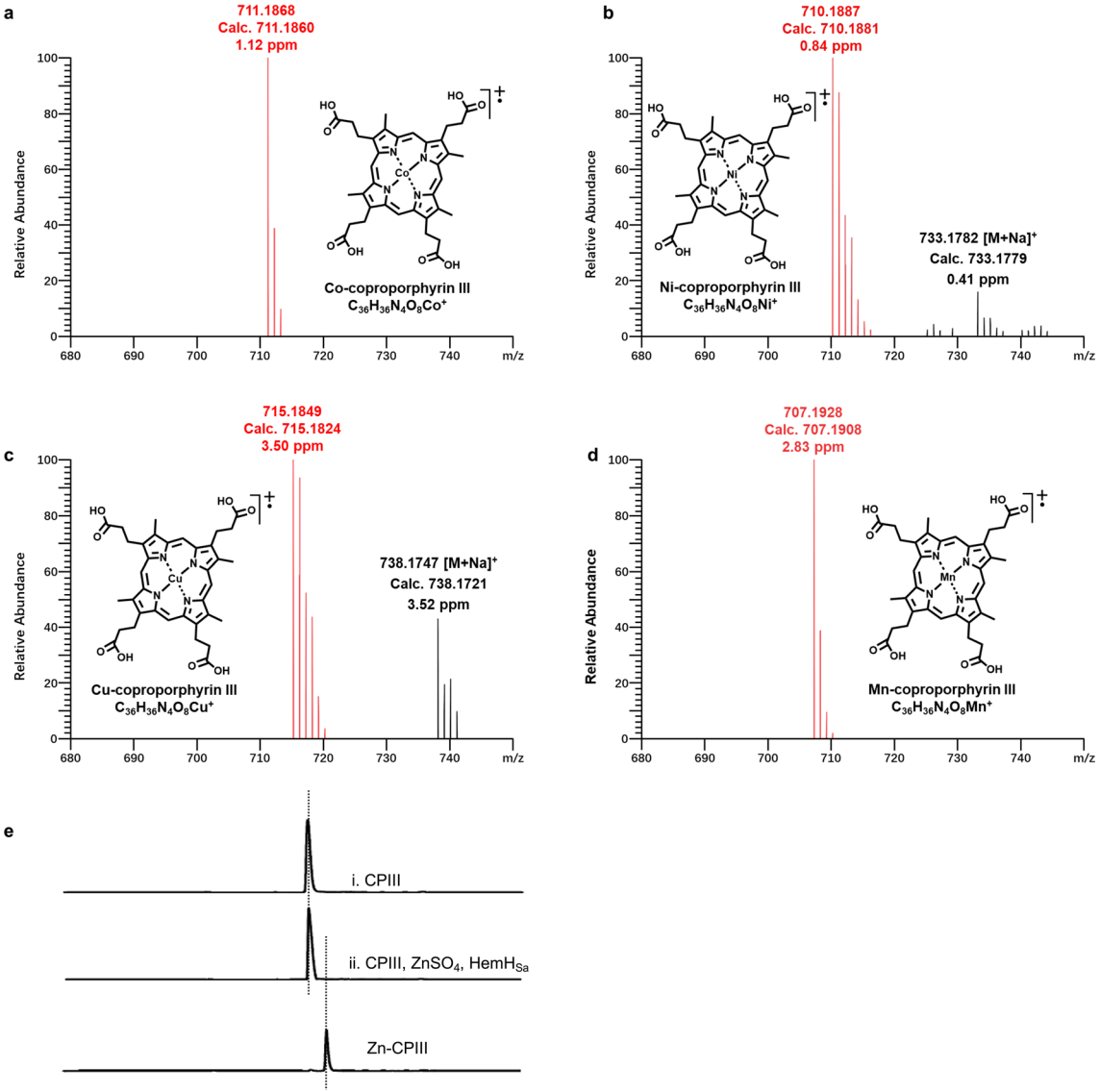
Extended Data Fig. 1 | Porphyrin pathway-derived products or intermediates and the verification of CPIII production in fermentation broth. a, The chemical structures of key products or intermediates in porphyrin biosynthetic pathway. 5-ALA, 5-Aminolevulinate; UPENIII, Uroporphyrinogen III; CPENIII, Coproporphyrinogen III; CPIII, Coproporphyrin III; Fe-CPIII, Fe-coproporphyrin III; VB_{12}, Vitamin B_{12}; PPIX, Protoporphyrin IX; Bchl, Bacteriochlorophyll. **b**, Structure verification of CPIII in fermentation broth sample. *i*) HPLC profile of sample and standard CPIII; *ii*) MS/MS spectra with 50-eV collision energy for purified and standard CPIII.

https://doi.org/10.1038/s41587-024-02267-3



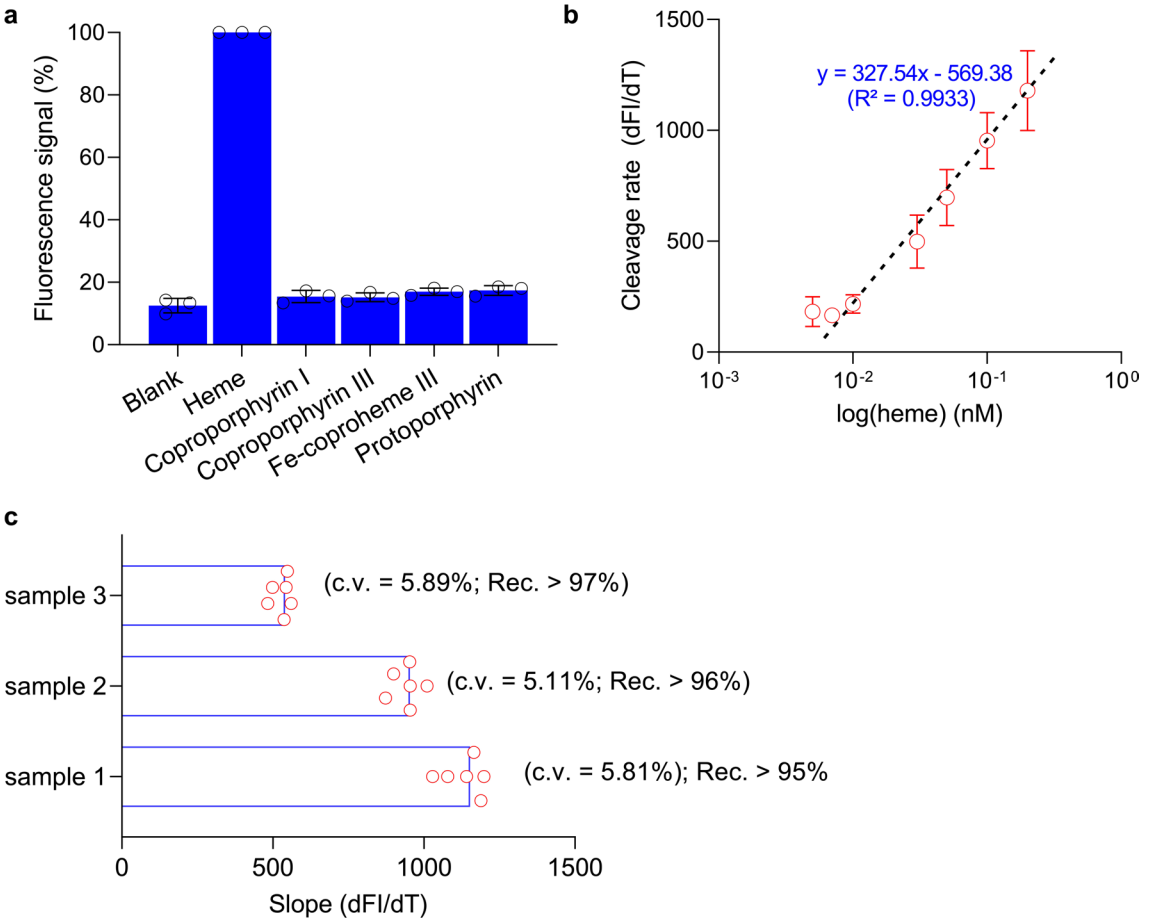
Extended Data Fig. 2 | Construction and PCR verification of various mutants and stepwise enhancement of CPIII production in *R. sphaeroides*. **a**, Construction and PCR verification 2.4.1-Δ*fnrL*. **b**, Construction and PCR verification of ZX-5-Δ*fnrL*. F1 and F2 are the PCR products that were amplified using ZX-5-Δ*fnrL*-up-ck-F/R and ZX-5-Δ*fnrL*-dn-ck-F/R, respectively. **c**. Construction and PCR verification of HY01-Δ*fnrL*. **d**. Construction and PCR verification of HY01-Δ*hemN*. F3 and F4 are the PCR products that were amplified using HY01-Δ*hemN*-up-ck-F/R and HY01-Δ*hemN*-dn-ck-F/R. **e**. Construction and PCR verification of HY01-Δ*hemN-prrAB*$_{pLB2}$. F5 and F6 are the PCR products that were amplified using Δ*hemN-prrAB*-up-ck-F/R and Δ*hemN-prrAB*-dn-ck-F/R. The PCR verifications in **b**-**c** were performed three times each ($n = 3$; replicates are shown in Source Data files; in each replicate, at least two double crossover conjugants were selected). **f**. Heat map depicts the differentially expressed PrrA target operons (selected) during fermentation in bioreactor at 16, 24, 40 and 60 h. This result indicated that three genes associated with the porphyrin metabolism pathway, namely *hemA*, *hemC*, and *hemE*, which are regulated by prrA, exhibited a substantial upregulation in transcription levels at the 40 h of fermentation compared to the 24 h. FPKM (fragments per kilobase of transcript per million fragments mapped) values were taken as generation of the heat map by origin 2022 software. **g**. Stepwise enhancement of CPIII production in *R. sphaeroides* (n = biologically independent replicates). *: Fed-batch fermentation in 5-L bioreactor; #: IPTG addition. Bar graph with error bars represents mean ± s. d.

https://doi.org/10.1038/s41587-024-02267-3



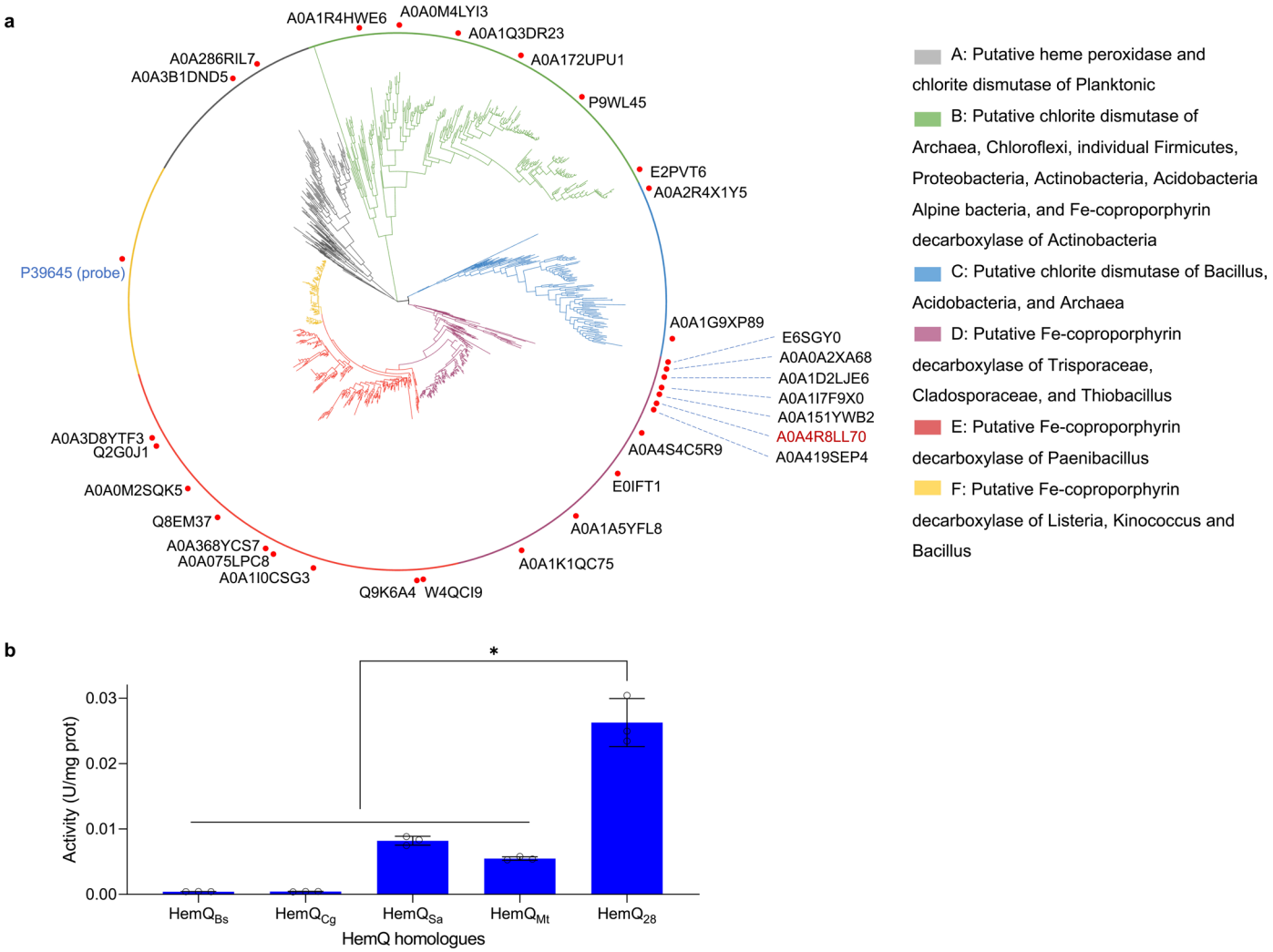
Extended Data Fig. 3 | Verification of metalloporphyrin production by HRMS and biocatalytic synthesis of Zincphyrin. a-d, Identification of Co-CPIII, Ni-CPIII, Cu-CPIII, and Mn-CPIII by high-resolution mass spectrometry (HRMS). All the accurate mass measurements for impurities were within < 5 ppm of the theoretical m/z value. **e**, HPLC profile of the enzymatic catalysis of CPIII for the *in vitro* synthesis of Zincphyrin using $HemH_{Sa}$ and zinc sulfate. The reaction is conducted in Tris-HCl buffer (pH 8.0) at 37 °C under the following conditions: i) In the reaction system, only 50 μM CPIII is present. ii) In condition i, 50 μM $ZnSO_4$ and 1 μM HemHSa were added.

https://doi.org/10.1038/s41587-024-02267-3



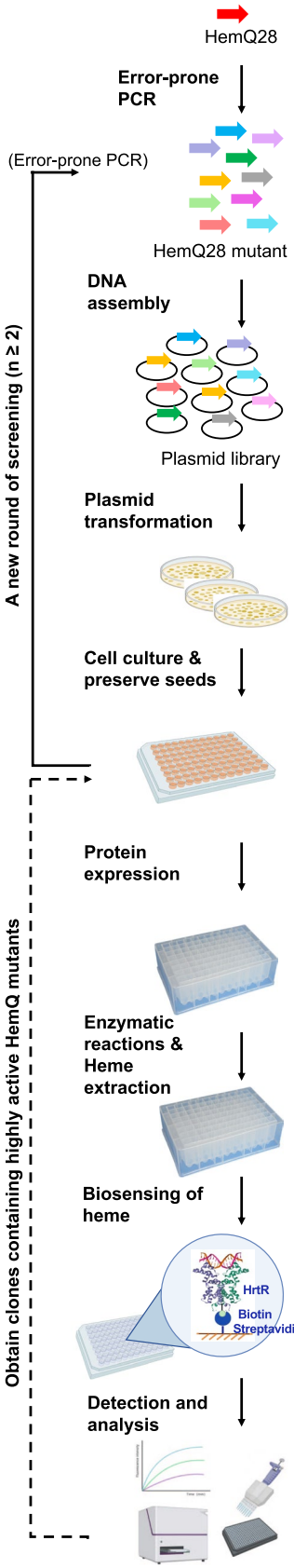
Extended Data Fig. 4 | Methodological characterization and analysis of CRISPR-Cas12a-based heme detection. a. Fluorescence intensity of detection system in the presence of heme and its structural analogues ($n = 3$ biological independent detection of fluorescence intensity per condition). Fluorescence intensity was measured in the presence of heme, coproporphyrin I, coproporphyrin III, Fe-coproheme III, and protoporphyrin, with a concentration of 200 nM for heme and 2000 nM for each of the remaining porphyrin compounds. **b.** The linear relationship between the concentration of heme and the cleavage rate. The concentration range in which the calibration curve was linear was 10–200 nM ($n = 3$ biological independent replicates; $R^2 > 0.993$). Bar graphs with error bars in **a** and **b** represent mean ± s. d. **c.** Analysis of the reproducibility and accuracy of heme detection method. Three different concentrations of heme samples (sample 1, 2, 3) were independently tested in six times ($n = 6$) using a 96-well plate. The coefficient of variation (c.v.) and sample recovery (Rec.) rate were calculated for the detection results.

https://doi.org/10.1038/s41587-024-02267-3



Extended Data Fig. 5 | Mining HemQ homologs and comparing crude enzyme activities. a. Mining of *hemQ* homologous (NCBI blast 2.11.0+) by using maximum likelihood method. The evolutionary history was inferred by using the Maximum Likelihood method and JTT matrix-based model. The tree with the highest log likelihood (−1234833.12) is shown. Initial tree(s) for the heuristic search were obtained automatically by applying Neighbor-Join and BioNJ algorithms to a matrix of pairwise distances estimated using the JTT model, and then selecting the topology with superior log likelihood value. The tree is drawn to scale, with branch lengths measured in the number of substitutions per site. This analysis involved 1000 amino acid sequences. There were a total of 1761 positions in the final dataset. Evolutionary analyses were conducted in MEGA X (version: 10.2.6). Utilizing *hemQ* from *Bacillus subtilis* (P39645) as a probe sequence, a total of 30 candidate genes were selected. The codon optimization and complete gene synthesis for the selected candidates were conducted by GenScript Inc (Nanjing, China). *E. coli* was employed for recombinant protein expression and subsequent activity assessment. **b**. The crude enzyme activity of $HemQ_{28}$ compared to different previously reported HemQ homologous proteins. $HemQ_{Bs}$, $HemQ_{Cg}$, $HemQ_{Sa}$, and $HemQ_{Mt}$ are derived from *Bacillus subtilis*, *Corynebacterium glutamicum*, *Staphylococcus aureus*, and *Mycobacterium tuberculosis*, respectively. All these proteins were recombinantly expressed in *E. coli* and prepared as corresponding crude enzyme solutions. The enzyme activity unit (U) was defined as the amount of enzyme required to catalyze the conversion of 1 μM substrate or generate 1 μM product within one minute under optimal temperature (37 °C) and pH conditions. This study used bovine serum albumin (BSA) at a known concentration as a reference and obtained bands of the target protein through SDS-PAGE. Subsequently, the concentration of the target protein was estimated by comparing its band intensities with those of BSA using BioRad Image Lab software (version: 6.0.0 build 25). Three biologically independent replicates ($n = 3$) were conducted for enzymatic activity detection of each HemQ homologue. Bar graph with error bars represent mean ± s. d. *$P < 0.05$.

https://doi.org/10.1038/s41587-024-02267-3



i) Random mutagenesis of *hemQ*$_{28}$ by error-prone PCR
S1: Using Takara's Diversify™ PCR Random Mutagenesis Kit (# 630703), perform error-prone PCR with the DNA sequence of hemQ28 as the template and Q28EP-F/R primers (F: 5'-gaaggagatatacatatgtcggcg-3'; R: 5'- tggtggtggtgctcgaggttgc-3').
S2: According to the kit's instructions, adjust the PCR conditions to achieve a mutation rate of 4.6 mutations per 1000 bp.

ii) Plasmid (or library) assembly
S3: Purify and recover the error-prone PCR product, and perform enzymatic digestion with restriction enzymes (XhoI and NcoI) on the PCR product and pET28a vector DNA.
S4: Using NovoRec® Plus PCR one-step assembly KIT (# NR005) to complete the DNA assembly and obtain a mutant plasmid library.

iii) Transformation of plasmid library into *E. coli*
S5: Thaw *Escherichia coli* BL21 (DE3) competent cells on ice. Add 20 μL of ligation product resulting from S4, 40 μL of 5×KCM*, and sterile water to make up the volume to 200 μL.
S6: Incubate the cells on ice for 30 minutes, heat shock at 42°C for 90 seconds, incubate on ice for an additional 2 minutes. Then, add 700 μL of LB medium and incubate at 37°C with 220 r.p.m. for 1 hour.
S7: Centrifuge at 5,000×g for 1 minute, discard the supernatant, and leave approximately 50 μL of LB medium in the Eppendorf tube.
S8: Resuspend the cells by pipetting, spread on a plate (Kan$^+$), and incubate overnight at 37°C.
(*5×KCM: Sodium chloride 3.73 g, calcium chloride 1.65 g, magnesium chloride 3.375 g, distilled water to make up to 100 mL, filter through a 0.22 μm sterile membrane, and store at -20°C.)

iv-i) Culture, protein expression, and then cell collection (Preserve seeds before induction)
S9: Pick single clones into a 96-well plate, with 150 μL of LB containing kanamycin (0.1%) per well, and incubate overnight at 37°C.
S10: Take an appropriate amount of culture and add glycerol (final concentration 10-15%) for seed preservation.

iv-ii) Culture, protein expression, and then cell collection (Preserve seeds before induction)
S11: Transfer 30 μL of the culture resulting from S9 to a deep well plate for protein expression.
S12: In each well of the deep-well plate, there is 1 mL of culture medium* for protein expression (0.1% kanamycin). After inoculation, cultivate at 37°C until reaching an OD of 0.4~0.8.
S13: Then, reduce the cultivation temperature to 16°C, after 48 hours of induction, centrifuge at 2190 g (Titan Scientific Lab, LDC-5) for 20 minutes to collect the cells.
(*100 ml culture medium includes: 95 ml of base medium (5 g/L yeast extract, 10 g/L peptone, 7.098 g/L Na_2HPO_4, 6.8045 g/L KH_2PO_4, 0.7102 g/L Na_2SO_4, 2.6745 g/L NH_4Cl, pH 7.5-8.0.), 5 ml of 20× carbon source solution (20 g/L glucose, 100 g/L glycerol, 200 g/L α-lactose.), 200 μl of 500× magnesium sulfate solution (120.37 g/L $MgSO_4$), and 100 μl of 50 mg/mL kanamycin.)

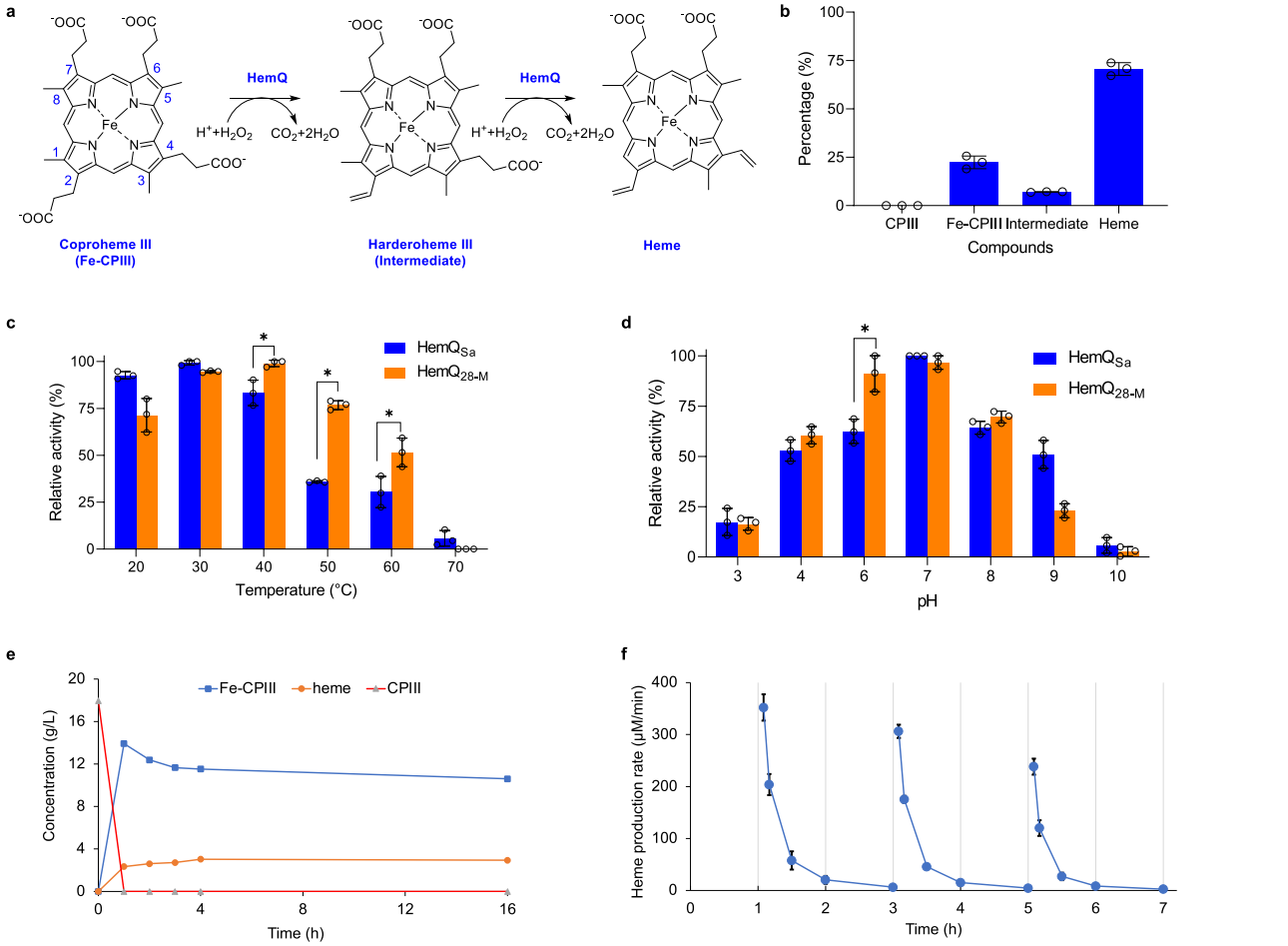
v) Add Fe-CPIII and buffer, incubation and then heme extraction
S14: Add 200 μl of cell lysis solution per well (containing 2 g/L lysozyme, 0.1% Triton X-100, pH 7.0 PBS) and lyse the cells at 37°C for 3 hours.
S15: Add 10 μl of substrate solution per well (5 μM Fe-CPIII) and incubate at 37°C for 40 minutes.
S16: Extract heme with 200 μl of 2% hydrochloric acid in acetone per well. After thorough mixing, add an additional 400 μl of PBS buffer (pH7.0) per well.

vi) Add heme extraction sample from v and incubation
S17*: Biotinylation of HrtR (refer to the Methods section) and immobilization of HrtR onto BeaverNano™ Streptavidin Matrix Coated 96-Well Plate (#22351; BEAVER, Suzhou, China).
S18*: Add 10 μL of 220 nM dsDNA solution to each well, incubate at room temperature for 30 minutes. Afterward, remove the liquid and wash each well three times with 200 μL of PBS (pH 7.0).
S19: Add 50 μL of the sample from S16 to each well, and incubate at 37°C for 10 minutes
(*These two steps can be prepared or prefabricated in advance. Refer to the Methods section.)

vii) Add reaction sample from vi (contains free activator dsDNA), Detection of fluorescence intensity(FI), Mutant screening and selection based on FI
S20*: Add 50 μL of detection buffer to each well in a 96-well plate, containing 5 μL of NEB 3.1 Buffer, 0.5 μL of 10 μM Cas12a, 0.5 μL of 10 μM crRNA, 1 μL of FQ-probe, and 33 μL of RNA-free water.
S21: Add 10 μL of the sample from S19, incubate at 37°C for 15-20 minutes.
S22: Detect the fluorescence signal using a microplate reader (excitation: 480 nm; emission: 520 nm; CLARIOstar, BMG LABTECH)
S23: Analyze the fluorescence intensity to screen for highly active HemQ mutants.
(*This step can be prepared or prefabricated in advance.)

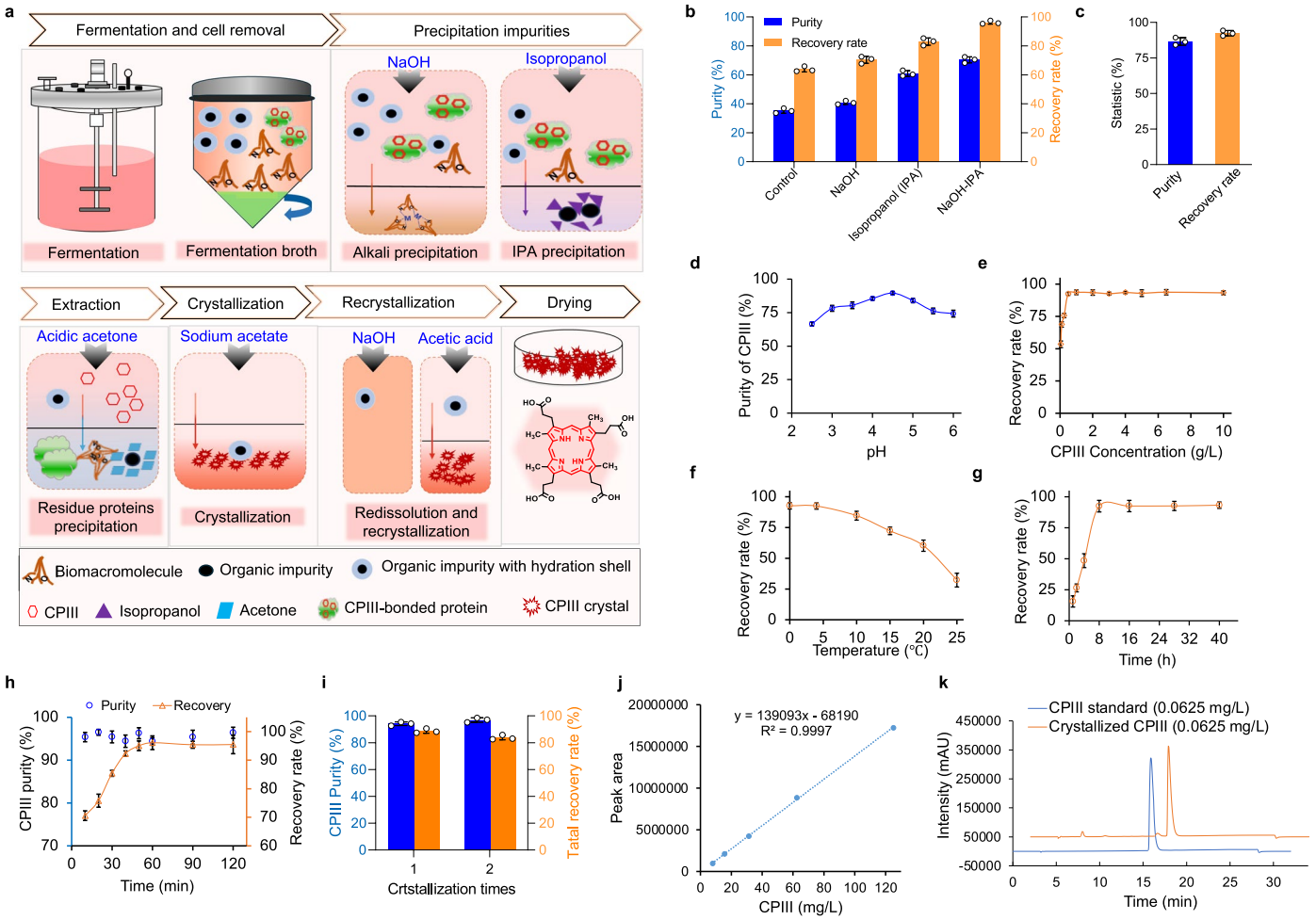
Extended Data Fig. 6 | Error-prone mutagenesis and screening of HemQ$_{28}$ variant. The process of mutation and screening includes: error-prone PCR, DNA assembly, plasmid transformation, cell culture and preservation, protein expression, enzymatic reaction and heme extraction, biosensing of heme, and detection and analysis.

https://doi.org/10.1038/s41587-024-02267-3



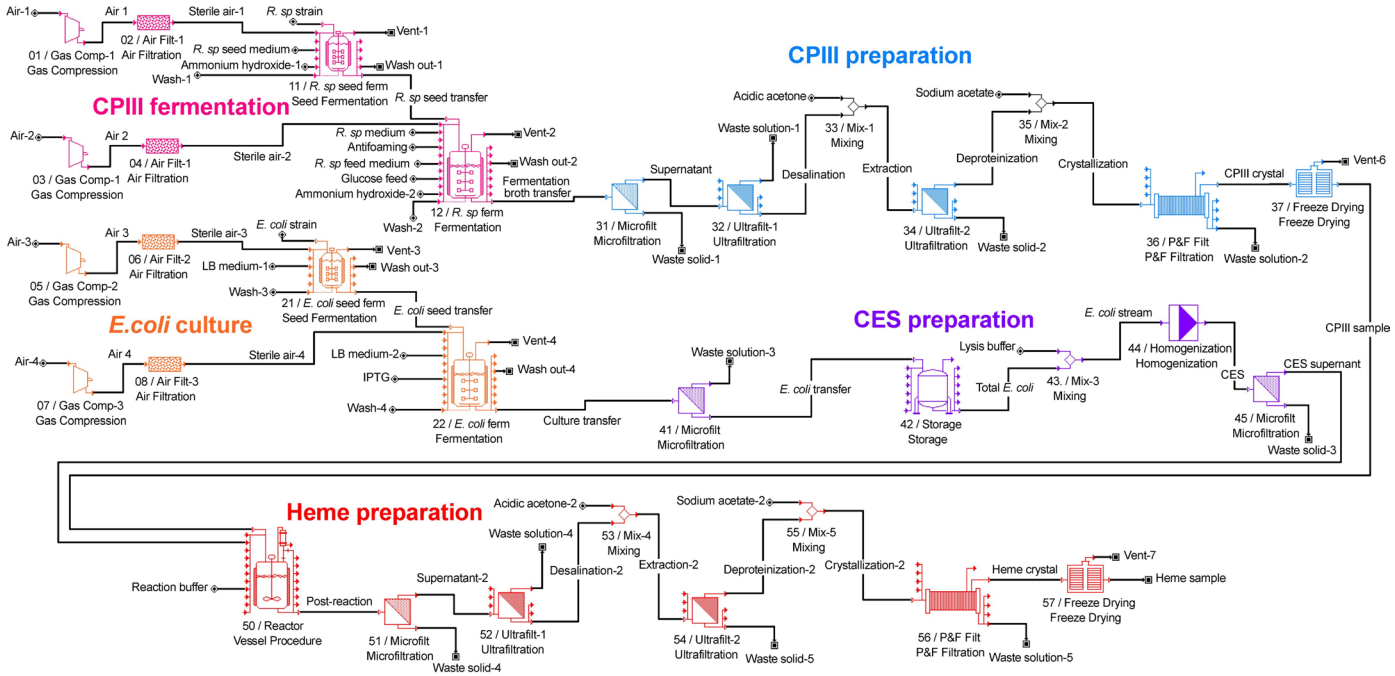
Extended Data Fig. 7 | Biocatalysis of heme by CPIII and the stability assessment of $HemQ_{28\text{-}M}$. **a**, **b**, Quantitative analysis of heme and other chemicals after enzymatic catalysis ($n = 3$ biologically independent replicates). **c**, **d**, Effects of temperature and pH on the enzymatic activity of $HemQ_{Sa}$ and $HemQ_{28\text{-}M}$. Three biologically independent replicates ($n = 3$) were conducted for each condition in **c** and **d**. **e**, One-time addition of crude enzyme catalyzed the conversion CPIII to heme in 5-L bioreactor. At the beginning of the reaction, 2 L of CPIII with a concentration of 18 g/L was added all at once. The crude enzyme supernatant obtained by crushing 180 g of wet recombinant *E. coli* cells was added to the reaction system at the beginning of the reaction (that is, 0 h). The reaction was performed at 37 °C and pH 7.0 with agitation at 100 rpm. **f**, Heme production rate after fed-batch addition of crude enzyme solution (CES) in 5-L bioreactor. After the enzymatic reaction commenced, the CES obtained by crushing wet recombinant *E. coli* cells was fed-batch added to the 5-L bioreactor at 1, 3, 5, and 7 h. This study measured the heme production rate within two hours after the addition of CES at 1, 3, and 5 h. The concentration of the target fusion protein in the CES was determined by comparing its band's grayscale intensity with that of a BSA standard following SDS-PAGE electrophoresis, using a concentration of 0.5 g/L BSA as a reference for quantification. Each addition of CES contains 722 ± 140 mg of target fusion protein (derived from approximately 36 g of wet *E. coli* cells). After each addition of CES, heme concentration increases were measured at five intervals (specifically, 0–5 min, 5–10 min, 25–30 min, 55–60 min, and 115–120 min) within the subsequent two hours to calculate the heme production rate for each corresponding time interval. Bar graphs with error bars represent mean ± s. d. *$P < 0.05$.

https://doi.org/10.1038/s41587-024-02267-3



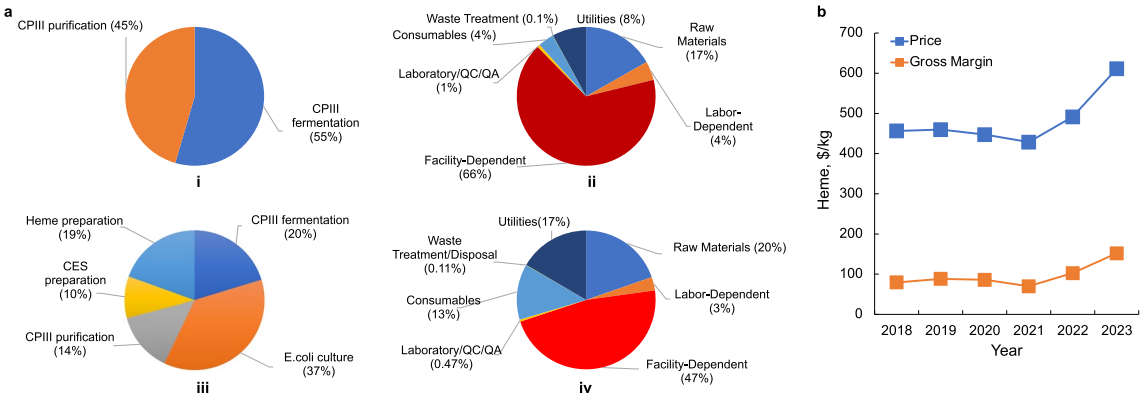
Extended Data Fig. 8 | Purification and preparation of CPIII from fermentation broth through crystallization. a, Proposed workflow for the purification and preparation of CPIII through crystallization. **b**, Effects of precipitation pretreatment on crystallization efficiency (three independent replicates were conducted under each condition). Control: direct crystallization using fermentation broth supernatant; NaOH: crystallization after alkaline precipitation (pH 8.5) using NaOH; IPA: addition of 20% isopropanol to the fermentation broth supernatant for alcohol precipitation followed by crystallization; NaOH-IPA: crystallization after combined alkaline and isopropanol precipitation. **c**, Effects of precipitation pretreatment and acidic acetone extraction on crystallization efficiency (three independent replicates were conducted under each condition). After combined alkaline precipitation and isopropanol precipitation (NaOH-IPA), the obtained supernatant undergoes crystallization following treatment with 30% acidic acetone. CPIII purity and recovery rates were calculated separately according to the Method section. **d**–**g**, Effect of pH, CPIII concentration, temperature, and crystallization time on the purity or recovery rate of CPIII. The CPIII fermentation broth supernatant was applied to optimized crystallization conditions. Purity and recovery rates were calculated separately following the procedures outlined in the Method section. **h**, Effects of recrystallisation time on the purity or recovery rate of CPIII. **i**, Effect of primary crystallization and recrystallization on the purity and recovery rate of CPIII (three independent replicates were conducted under each condition). CPIII purity and recovery rates were calculated separately according to the Method section. **j**, The HPLC quantitative standard curve for CPIII. CPIII standard (#C882263; Macklin3 Inc, Shanghai, China) of 1 mg was dissolved in 1 mL of DMSO to prepare a stock solution with a concentration of 1000 mg/L. Under subdued light conditions, the CPIII stock solution was further diluted in a series of concentrations using DMSO, resulting in solutions with concentrations of 125 mg/L, 62.5 mg/L, 31.25 mg/L, 15.625 mg/L, and 7.8125 mg/L. Each concentration was prepared in triplicate. The peak areas of CPIII at 390 nm were determined using HPLC. The peak area values were obtained for each concentration, and the data represent mean ± s. d. of three replication. **k**, The HPLC profiles of purified CPIII sample and the CPIII standard. Based on the CPIII standard curve calculation, the purity of CPIII samples was determined to be 95.2%.

https://doi.org/10.1038/s41587-024-02267-3



Extended Data Fig. 9 | Simulation of large-scale CPIIII and heme bioproduction processes for techno-economic analysis. This model is designed to simulate the large-scale production of CPIII crystals (with a CPIII content of at least 95%, w/w) and heme crystals (with a heme content of at least 93%, w/w). The process for CPIII production consists of two sections: CPIII fermentation for obtaining CPIII fermentation broth, and CPIII preparation for obtaining CPIII crystal product via purification and crystallization. The annual production rate is 20 tons of CPIII. According to the model, the installation is planned to operate 24 hours a day, for a total of 329 days per year (the remaining days were allocated for maintenance and conservation tasks). The annual batch throughput for producing heme is 69 batches, with each batch time and cycle time is 127 and 114 h, respectively. The process for heme production comprises five sections: CPIII fermentation to obtain CPIII fermentation broth (shared with CPIII production), CPIII preparation to obtain CPIII crystal products through purification and crystallization (shared with CPIII production), *E. coli* culture to cultivate *E. coli* cells expressing recombinant fusion proteins in fermenters, CES preparation involves cell storage and disruption to obtain cell lysate supernatant containing recombinant fusion proteins, and the Heme preparation section to catalyze the conversion of CPIII into heme using CES and subsequently purify and crystallize to obtain the final heme product (crystallization and purification equipment and lines are shared with CPIII production). The annual production rate is 16 tons of heme. According to the model, the installation is planned to operate 24 hours a day, for a total of 330 days per year (the remaining days were allocated for maintenance and conservation tasks). The annual batch throughput for producing heme is 69 batches, with each batch time and cycle time is 148 and 114 h, respectively. The modeling process utilizes parameters or data from both the built-in database of SuperPro® Designer simulation software and project-specific data from both the experimental results of this study and the Supplementary Table. 4.

https://doi.org/10.1038/s41587-024-02267-3



Extended Data Fig. 10 | Techno-economic analysis of large-scale CPIII and heme bioproduction. a, Breakdown of annual operating cost for CPIII and heme production. i, Annual cost breakdown by section (%) for CPIII production. ii, Annual operating cost breakdown (%) for CPIII production. iii, Annual cost breakdown by section (%) for heme production. iv, Annual operating cost breakdown (%) for heme production. In this model, the total annual operating costs for CPIII and heme are $935,000 and $2,512,000, respectively (Supplementary Table. 5). The data in panels i and iii are derived from Itemized Cost analyses conducted within this model, while the data in panels ii and iv stem from the Economic Evaluation analysis. The facility-dependent cost encompasses expenses for maintenance, depreciation, and miscellaneous costs. Labor-Dependent Cost: comprises all labor-dependent operating expenses excluding those for laboratory analyses, quality control, and quality analyses. Laboratory/QC/QA Cost: covers laboratory analyses, quality control, and quality analyses. Consumables Cost: certain equipment necessitates the use of consumables; this cost category includes expenses for periodically replaced materials. Utilities: Heating Agents, Cooling Agents, and Power Types. The modeling process utilizes parameters or data from both the built-in database of SuperPro® Designer simulation software and project-specific data from both the experimental results of this study and the Supplementary Table. 4. **b**. The annual average price and gross margin of heme in the international trading market over the last six years (2018–2023). The information related to the price and gross margin of heme in the international trading market is based on the 2023 Heme Market Research Report, a commercially available market research report provided by MARKET MONITOR Co., Ltd, Changsha, China. The Market Research Report was published on July 15, 2023, with the report code GMM2292280. For more details, please visit the webpage: https://www.globalmarketmonitor.com.cn/reports/2292280-hemoglobin-market-report.html.

nature research

Corresponding author(s): Gao-Yi Tan, Lixin Zhang

Last updated by author(s): Apr 23, 2024

Reporting Summary

Nature Research wishes to improve the reproducibility of the work that we publish. This form provides structure for consistency and transparency in reporting. For further information on Nature Research policies, see Authors & Referees and the Editorial Policy Checklist.

Statistics

For all statistical analyses, confirm that the following items are present in the figure legend, table legend, main text, or Methods section.

n/a	Confirmed	
☐	☒	The exact sample size (*n*) for each experimental group/condition, given as a discrete number and unit of measurement
☐	☒	A statement on whether measurements were taken from distinct samples or whether the same sample was measured repeatedly
☐	☒	The statistical test(s) used AND whether they are one- or two-sided *Only common tests should be described solely by name; describe more complex techniques in the Methods section.*
☒	☐	A description of all covariates tested
☐	☒	A description of any assumptions or corrections, such as tests of normality and adjustment for multiple comparisons
☐	☒	A full description of the statistical parameters including central tendency (e.g. means) or other basic estimates (e.g. regression coefficient) AND variation (e.g. standard deviation) or associated estimates of uncertainty (e.g. confidence intervals)
☐	☒	For null hypothesis testing, the test statistic (e.g. *F*, *t*, *r*) with confidence intervals, effect sizes, degrees of freedom and *P* value noted *Give P values as exact values whenever suitable.*
☒	☐	For Bayesian analysis, information on the choice of priors and Markov chain Monte Carlo settings
☒	☐	For hierarchical and complex designs, identification of the appropriate level for tests and full reporting of outcomes
☒	☐	Estimates of effect sizes (e.g. Cohen's *d*, Pearson's *r*), indicating how they were calculated

Our web collection on statistics for biologists contains articles on many of the points above.

Software and code

Policy information about availability of computer code

Data collection	Gel Image: Tanon Gel Imaging System (version: Tanon 1600) or ChemiDocTM XRS+ Imaging System (Bio-Rad) Fluorescence intensity: BMG LABTECH, CLARIOstar (Software version: 5.20 R5, Firmware version: 1.16) Chemical Structure: Cambridge Soft, ChemBioDraw Ultra (Version:12.00) HPLC: Agilent Technologies OpenLAB CDS ChemStation Edition for LC & LC/MS Systems (Version: C.01.07 SR2 [255]) HRMS & MS/MS: Thermal UltiMate 3000 UHPLC coupled with Thermo Scientific Q Exactive Orbitrap mass spectrometer 5-L bioreactor: Bailun Biochemical Technology, BLBIO-5GJ-3 200-L bioreactor: SHANGHAI BAOXING BIO ENGING EQUIPMENT, BIOTECH-3000 crRNA design: Python (Software version:3.8) HemQ homologous mining: NCBI blast 2.11.0+
Data analysis	Gel Image analysis: BioRad, Image Lab (version: 6.0.0 build 25) Fluorescence intensity analysis: BGM LABTECH, MARS data analysis software (version: 3.20. R2) Data analysis: Microsoft Office Home & Student 2016 - Excel & Graphpad Prism 9 (version: 9.5.1; GraphPad Software, LLC) HPLC data analysis: Agilent OpenLAB CDS ChemStation Edition (Version: C.01.10 [201]) HRMS & MS/MS: Thermo Xcalibur Qual Browser (Software version:3.1) Michaelis-Menten equation fitting: Graphpad Prism (version 9.5.1; GraphPad Software, Inc.) Heat map analysis: Origin 2022 Evolutionary analyses: MEGA X (version: 10.2.6); BioNJ algorithms Techno-economic analysis: SuperPro® Designer V10.7 simulation software (Intelligen, Inc.)

For manuscripts utilizing custom algorithms or software that are central to the research but not yet described in published literature, software must be made available to editors/reviewers. We strongly encourage code deposition in a community repository (e.g. GitHub). See the Nature Research guidelines for submitting code & software for further information.

Data

Policy information about availability of data

All manuscripts must include a data availability statement. This statement should provide the following information, where applicable:

- Accession codes, unique identifiers, or web links for publicly available datasets
- A list of figures that have associated raw data
- A description of any restrictions on data availability

The authors declare that the primary data supporting the findings of this study are accessible within the paper and its Supplementary Information files. Source data are provided with this paper, and additional data can be obtained from the corresponding author upon request.

Field-specific reporting

Please select the one below that is the best fit for your research. If you are not sure, read the appropriate sections before making your selection.

☒ Life sciences ☐ Behavioural & social sciences ☐ Ecological, evolutionary & environmental sciences

For a reference copy of the document with all sections, see nature.com/documents/nr-reporting-summary-flat.pdf

Life sciences study design

All studies must disclose on these points even when the disclosure is negative.

Sample size	For the genetic engineering of Rhodobacter sphaeroides, 2-4 double crossover conjugants were selected for subsequent study. For CPIII fermentation in 5L and 200L bioreactors, approximately twenty time-points covering all stages of fermentation were analyzed. For CPIII isolation and purification from fermentation broth, three biological replicates were performed. For all other experiments, three biological replicates were conducted to calculate average values and standard deviations.
Data exclusions	No date was excluded from the analyses.
Replication	At least three biological replicates were utilized in the quantitative analysis experiment (e.g. Fig.1f; Fig. 2c, e; Fig. 4b, d; Fig. 5f; Fig. 6f, g; Extended Data Fig. 4a, b, c; Extended Data Fig. 5b; Extended Data Fig. 7b, c, d; Extended Data Fig. 8b, c, d, e, f, g, h, i). The electrophoresis experiment (including agarose gel electrophoresis and SDS-PAGE) was repeated three times. All attempts at replication were successful.
Randomization	This study aims to engineer and identify superior microorganisms and enzymes for the efficient production of target compounds, addressing industrial demands. During the screening of microbial strains and enzymes, the objective is to identify strains with more pronounced color phenotypes and enzymes capable of producing stronger fluorescence. Therefore, randomization has not be the primary consideration.
Blinding	The subjects of this study were microorganisms and compounds, blinding was not relevant to this study.

Reporting for specific materials, systems and methods

We require information from authors about some types of materials, experimental systems and methods used in many studies. Here, indicate whether each material, system or method listed is relevant to your study. If you are not sure if a list item applies to your research, read the appropriate section before selecting a response.

Materials & experimental systems

n/a	Involved in the study
☒	☐ Antibodies
☒	☐ Eukaryotic cell lines
☒	☐ Palaeontology
☒	☐ Animals and other organisms
☒	☐ Human research participants
☒	☐ Clinical data

Methods

n/a	Involved in the study
☒	☐ ChIP-seq
☒	☐ Flow cytometry
☒	☐ MRI-based neuroimaging